Scavenging of Uranium in Experimental and Natural Samples

KAN LI

B.Eng. (2007), Shanghai University, Shanghai, China

M.Eng. (2010), The University of Adelaide

This thesis is submitted for the degree of Doctor of Philosophy
in
School of Chemical Engineering
at
The University of Adelaide

THE UNIVERSITY
of ADELAIDE

January 2016
Adelaide, Australia

Table of Contents

Abstract

The hypothesis that interface coupled dissolution-reprecipitation reactions (ICDR) can play a key role in scavenging minor elements has been investigated via exploring the fate of U during the experimental sulfidation of hematite to chalcopyrite and the exsolution of chalcopyrite from bornite digenite solid solution (*bdss*) under hydrothermal conditions. The results of experiments with two kinds of Uranium (U) sources; either as solid UO_{2+x}(s) or as a soluble uranyl complex, differed from the U-free experiments. In the reactions from hematite to chalcopyrite under 220-300 ^{o}C hydrothermal conditions, pyrite precipitated initially, before the onset of chalcopyrite precipitation. In addition, when UO_{2+x}(s) was included in the experiments, enhanced hematite dissolution led to increased porosity and precipitation of pyrite+magnetite within the hematite core. However, in uranyl nitrate bearing experiments, abundant pyrite formed initially, before being replaced by chalcopyrite. Uranium scavenging was mainly associated with the pyrite precipitation, as a result that a thin U-rich layer along the original hematite grain surface precipitated out. In the reactions of chalcopyrite exsolution from *bdss* during annealing under hydrothermal conditions in a solutions nominally containing Cu(I) and hydrosulfide in a $pH_{25^{\circ}C}$ ~6 acetate buffer, a similar U-rich rim was observed along the original grain when uranyl nitrate as U-source was included in the reactions. The precipitation of uranium was related to the presences of HS^{-} in buffer. Chemical mapping and X-ray absorption near edge structure (XANES) spectroscopy showed the UO_{2+x}(s) was the mainly restricted to the U-rich layer. The two sets of experiments demonstrate that the presence of minor components can affect the pathway of ICDR reactions. Reactions between U- and Cu-bearing fluids and hematite or chalcopyrite can explain the Cu-U association prominent in some iron oxide-copper-gold (IOCG) deposits.

In this study, synchrotron-based X-ray fluorescence (SXRF) mapping was used to trace the distribution of uranium in natural samples from different geological contexts (sandstone-hosted U-deposit; IOCG) for investigating the deportment of uranium and its paragenesis in the context of thin-section scale textural complexity. It has been confirmed that the enrichment of U occurs via late dissolution-reprecipitation reactions in the bornite ores of the Moonta and Wallaroo IOCG deposits (South Australia), and that the U distribution in the ores of sandstone-hosted U-deposit is complex. Image analysis also revealed a number of new results for other minor elements, e.g. (i) the distribution of μm-sized Pt-rich grains and evidence for Ti-mobility during the formation of schistosity at the Fifield Pt prospect (New South Wales, Australia); (ii) the presence of Ge contained in organic matter and of Hg minerals associated within quartzite clasts in the Lake Frome U ores (South Australia); and (iii) confirmation of the two-stage Ge-enrichment in the Barrigão deposit, with demonstration of the presence of Ge in solid solution in the early chalcopyrite (Portuguese Iberian Pyrite Belt).

Declaration

I certify that this work contains no material which has been accepted for the award of any other degree or diploma in my name, in any university or other tertiary institution and, to the best of my knowledge and belief, contains no material previously published or written by another person, except where due reference has been made in the text. In addition, I certify that no part of this work will, in the future, be used in a submission in my name, for any other degree or diploma in any university or other tertiary institution without the prior approval of the University of Adelaide and where applicable, any partner institution responsible for the joint-award of this degree.

I give consent to this copy of my thesis when deposited in the University Library, being made available for loan and photocopying, subject to the provisions of the Copyright Act 1968.

The author acknowledges that copyright of published works contained within this thesis resides with the copyright holder(s) of those works.

I also give permission for the digital version of my thesis to be made available on the web, via the University's digital research repository, the Library Search and also through web search engines, unless permission has been granted by the University to restrict access for a period of time

Signature: Date: 03-Jan-2016

Acknowledgements

Firstly, I would like to thank my supervisors Prof. Joël Brugger, Prof. Allan Pring, A/Prof. Yung Ngothai, A/Prof. Antony Hooker and A/Prof. Brain O'Neill for introducing me to this exciting and great project. Without their endless support, encouragement, enthusiams and numerous invaluable advices over the last 4 years, I would never have obtained the success of this project.

I am particularly grateful to Dr. Barbara Etschmann of Monash University who went through all the detail to clarify many points in the experiments and the published papers. She constantly encouraged and motivated me and was always available to share problems and success. My sincere thanks also go to Dr. Fang Xia, Dr. Jing Zhao, Dr. Yuan Mei and Dr. Yuan Tian for their assistance in conducting experiments and many insightful suggestions, to Mr. Michael Jung and Mr. Jason Peak of Chemical Engineering Workshop for building and maintaining the hydrothermal apparatus, to Mr. Ben McHenry of South Australian Museum for prompt responses to requests for chemicals and lab equipments, to Dr. Animesh Basak, Dr. Benjamin Wade, Ms. Aoife McFadden and Mr. Angus Netting of Adelaide Microscopy for their technical assistance with FESEM, FIB/SEM, and EPMA, and to Dr. Artem Borysenko and Mr. Andrew Ostrowski of EPA, South Australia for their technical support on testing the radioactivity of uranium samples. I also acknowledge Dr. Fred Mosselmans of Diamond Light source, UK and Dr. Daryl Howard of Australian Synchrotron for helping me with my synchrotron experiments.

I would also like to thank Australian Department of Education and Training, for providing me the scholarship of Australian Postgraduate Award. This project has been made possible

by the financial support from the Institute for Mineral and Energy Resources (IMER) and the Australian Research Council (grant DP1095069 and DP1093238).

Finally, I thank my parents for their continual support and understanding. I would like to share this gorgeous moment with my wife, Lu Yu and my daughter, Alice Li, who deserves special thanks for always being supportive. Furthermore, I would also like to thank my friends, Kaiyue Lu, Chenling lv and Xiao Wang, for your endless support. I love you all and I am going to make you proud.

List of publications

This PhD thesis is of publication format. Three papers constructed this PhD thesis, including

ONE PUBLISHED PAPER

1 **Kan Li;** Allan Pring; Babara Etschmann; Edeltraud Macmillan; Yung Ngothai; Brain O'Neill; Anthony Hooker; Fred Mosselmans; Joel Brugger, Uranium scavenging during mineral replacement reactions, *American Mineralogist,* 2015, 100, 8-9: 1728-1735

ONE ACCEPTED MANUSCRIPT:

2 **Kan Li**; Barbara Etschmann; Nicholas Rae; Frank Reith; Chris G. Ryan; Robin Kirkham; Daryl Howard; Diogo R.N. Rosa; Carla Zammit; Allan Pring; Yung Ngothai; Antony Hooker; Joël Brugger, Ore petrography using megapixel X-ray imaging: Rapid insights into element distribution and mobilisation in complex Pt and U-Ge-Cu ores, accepted pending revisions in *Economic Geology*

ONE MANUSCRIPT IN DRAFT:

3 **Kan Li;** Joël Brugger; Yung Ngothai; Allan Pring, The exsolution of chalcopyrite from bornite digenite solid solution under hydrothermal conditions: an example of a back replacement reaction, to be submitted to a geochemistry journal.

OTHER PUBLICATIONS RELATED TO THIS THESIS:

REFEREED JOURNAL PAPERS

A Carla Zammit; **Kan Li**; Barbara Etschmann; Joël Brugger; Frank Reith, Geobiology of *in situ* uranium leaching, Advanced Materials Research, 2013, 825, 372-375

B Victor M. Okrugin; Elena Andreeva; Barbara Etschmann; Allan Pring; **Kan Li**; Jing Zhao; Grant Griffiths; Gregory R. Lumpkin; Gerry Triani; Joël Brugger, Microporous gold: Comparioson of textures from nature and experiments, *American Mineralogist,*

2014, 99, 1171-1174

REFEREED CONFERENCE PAPER

C Jing Zhao**;** Allan Pring; Joël Brugger; Fang Xia; **Kan Li;** Yung Ngothai, Hydrothermal mineral replacement reactions and their applications in mining and processing, *5th International Seminar on Process Hydrometallurgy, 2013, Santiago, Chile*

Chapter 1

Introduction

1.1 Uranium Production in Australia

In Australia, uranium has been mined and treated commercially since 1954. Radium Hill in South Australia, Rum Jungle in Northern Territory, and Mary Kathleen in Queensland, were the largest producers of uranium products (as yellowcake U_3O_8) until 1971 (Mudd, 2008). During that period the uranium produced was mainly intended for USA and UK weapons' programs, but some was used to fuel reactors for power generation. With the development of civil nuclear power, the production of Uranium (U_3O_8) in Australia significantly increased up to 11,217 tonnes per annum in 2005 (Mudd, 2008). Although Australia is essentially a nuclear-free country, the known uranium resources are the world's largest with some ~31% of the world total economic reserves; and it is also the world's third-ranking producer, behind Kazakhstan and Canada in 2014 (Association, 2014). Table 1.1 summarizes the recent production from individual mines in Australia.

Table 1.1 Uranium Production from Individual Mines (tonnes of U_3O_8)

	2007-08	2008-09	2009-10	2010-11	2011-12	2012-13	2013-14	2014-15
Ranger	5273	5678	4262	2677	3284	4313	1113	2044
Olympic Dam	4115	3974	2258	4012	3853	4064	3988	3144
Beverley	707	626	630	347	413	453	188	0
Four Mile					0	0	186	922
Honeymoon			0	0	151	124	37	0
Total	10,095	10,278	7150	7036	7701	8964	5512	6110

Note: All data came from http://www.world-nuclear.org/info/Country-Profiles/Countries-A-F/Australia/

With the exception of the Ranger mine, all other four operating mines are located in South Australia (Fig. 1.1). Olympic Dam, as the largest known uranium orebody in the world, is with U_3O_8-production ranging from 1800 to 4600 tonnes annually. About 80% of the uranium is recovered by conventional acid leaching of the flotation tailings from copper recovery, and the other 20% is from acid leach of the copper concentrate (BHP Billiton, 2011).

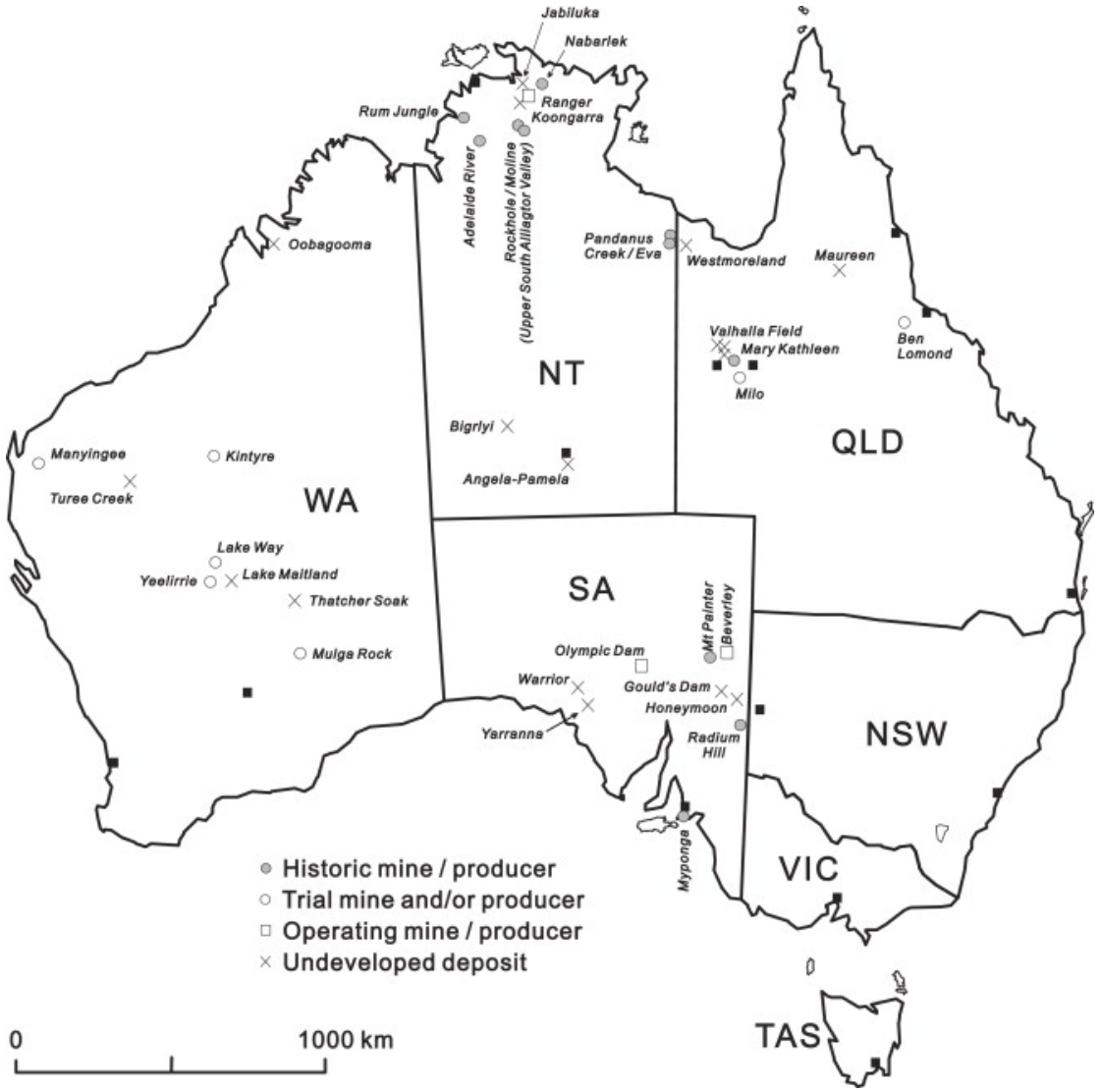

Figure 1.1 Map of uranium mines in Australia (after (Mudd, 2008))

The Beverley mine in South Australia, commenced operation in late 2000, was Australia's first *in situ* leach mine, accessing a palaeochannel deposit in sands in a saline aquifer (Taylor et al., 2004). In 2004, the production of U_3O_8 reached to 1180 tonnes at the mine. In the last two years of operation, almost all production through the Beverley plant came from the North orebody, which is contiguous with the Four Mile deposits. Mining of Beverley ceased at the end of 2013, and of Beverley North early in 2014. In 2014, production commenced on the Four Mile leases continuing on from Beverley operation, also via *in situ*

leaching. Uranium recovery is through Heathgate's Pannikin satellite ion exchange plant. The loaded resin then trucked to the main Beverley plant for stripping (elution) and precipitation. Production is predicted to reach to around 800 tonnes of U_3O_8 per year (Association, 2014). The Honeymoon mine in South Australia commenced operation in 2011, and is also an *in situ* leaching mine, and operations are ramping up to 400 tonnes/year. In November 2013, the mine was closed; and was put on care and maintenance, due to the fall in commodities prices (Birch et al., 2013).

1.2 Uranium Ores Deposits

In South Australia, uranium ores deposits fall into two geological types: sandstone deposits (e.g. Beverley, Four Mines, and Honeymoon), and iron-ore-copper-gold (IOCG)-U (e.g. Olympic Dam) according to the classification from International Atomic Energy Agency (IACE) (Ceyhan, 2009).

Sandstone deposits are contained within medium to coarse-grained sandstones deposited in a continental fluvial or marginal marine sedimentary environment. Impermeable shale or mudstone units are interbedded in the sedimentary sequence and often occur immediately above and below the mineralised horizon (Ceyhan, 2009). Uranium is mobile under oxidising conditions (U^{6+}) and precipitates under reducing conditions (U^{4+}), and thus the presence of a reducing environment is essential for the formation of uranium deposits in these sandstone systems. The basal channel (palaeochannel) deposit is one sub-type of the broad group of sandstone deposits, and the Honeymoon, Beverley and Four Mine are of this basal channel type. These deposits are hosted in palaeochannels filled with Cainozoic sediments and the source of their uranium is proposed to be from the uranium-rich Palaeo- to Mesoproterozoic rocks of the Mount Painter Inlier (Jaireth et al., 2010).

The other uranium deposit type in South Australia is the breccia complex deposit (iron-ore-copper-gold (IOCG) deposit), of which Olympic Dam is also the only deposit of this type known to contain economically significant quantities of uranium. Olympic Dam in South Australia is the world's largest resource of low-grade uranium (McKay and Miezitis, 2001) and accounts for about 66% of Australia's reserves (Ceyhan, 2009). Uranium occurs with copper, gold, silver, and rare earth elements (REE) in a large hematite-rich granite breccia complex in the Gawler Craton overlain by approximately 300 metres of flat-lying sedimentary rocks of the Stuart Shelf. Another example for the Breccia type is the Mount Gee area in the Mount Painter Inlier, South Australia. Uranium mineralised quartz-hematite breccia are related to Palaeoproterozoic granites with uranium contents of up to 100 ppm (Idnurm and Heinrich, 1993). Hydrothermal processes at about 300 million years ago remobilised uranium from these granites and enriched them in the quartz-hematite breccias. The breccias in the area host a low grade resource of 31,400 t U_3O_8 at 615 ppm (Weisheit et al., 2013).

1.3 Uranium Minerals

Table 1.2 lists most of uranium primary and secondary minerals. The major primary ore mineral is uraninite ($(U,Pb, Ca,Y,REE)O_{2+x}$), though a range of other uranium minerals are found in particular deposits. Coffinite ($U(SiO_4)_{1-x}(OH)_{4x}$), and brannerite ($(U,Ca,Y,Ce)(Ti, Fe)_2O_6$) are two other dominant Uranium minerals. In Olympic Dam, the grain size of the uranium minerals varies from submicron to several millimeters; but most of the grains are less than 50 µm in size. The current understanding is that uraninite is more strongly associated with hematite than with non-hematite gangue or sulphides, whilst brannerite and coffinite are more commonly associated with non-hematite gangue than with hematite or sulphides. The sulphides and gangue minerals do not appear to have been affected by

multiple cycles of dissolution and reprecipitation. Brannerite is restricted in its distribution and commonly occurs in veins in the Brooks Member of the Olympic Dam Formation. It is closely associated with rutile (anatase), and sericite. The brannerite grains are always surrounded by a halo of small (1 to 10 μm) grains of titanium oxide (rutile, anatase). At a more fundamental level, the formation of IOCG deposits is controlled by the properties of the minerals paragenises.

An understanding of the process of uranium minerals formation, combined with a detailed knowledge of the local geology, brings the ability to better explain the formation of IOCG deposits, and predict the distribution and grade of ores. This should lead to improvements in the efficiency of mining, ore treatment, and tailings management.

Table 1.2 List of the principal Uranium Minerals known from Australian deposit

	Name	**Chemical Formula**
Primary	Uraninite	$(U,Pb, Ca,Y,REE)O_{2+x}$
	Coffinite	$U(SiO_4)_{1-X}(OH)_{4X}$
	Brannerite	$(U,Ca,Y,Ce)(Ti, Fe)_2O_6$
	Davidite	$(REE)(Y,U)(Ti,Fe3+)_{20}O_{38}$
	Thucholite	Uranium-bearing pyrobitumen
Secondary	Autunite	$Ca(UO_2)_2(PO_4)_2$ x 8-12 H_2O
	Carnotite	$K_2(UO_2)_2(VO_4)_2$ x 1–3 H_2O
	Gummite	Gum mixture of various uranium minerals
	Saleeite	$Mg(UO_2)_2(PO_4)_2$ x 10 H_2O
	Torbernite	$Cu(UO_2)_2(PO_4)_2$ x 12 H_2O
	Tyuyamunite	$Ca(UO_2)_2(VO_4)_2$ x 5-8 H_2O
	Uranocircite	$Ba(UO_2)_2(PO_4)_2$ x 8-10 H_2O
	Uranophane	$(UO_2)_2(HSiO_4)_2$ x 5 H_2O
	Zeunerite	$Cu(UO_2)_2(AsO_4)_2$ x 8-10 H_2O

1.4 Mineral Replacement and Coupled Dissolution Reprecipitation Mechanism

Mineral replacement reactions can occur whenever a mineral is not in equilibrium with the surrounding fluids (Putnis and Mezger, 2004). Processes such as cation exchange, chemical weathering, deuteric alteration, pseudomorphism and leaching, are all linked by common

features in which one mineral or mineral assemblage is replaced by a more stable assemblage (Putnis, 2002). Numerous examples of mineral replacement reactions have been reported, such as the transformation from leucite to analcime (Putnis et al., 2007), the replacement of pentlandite by violarite (Xia et al., 2009a), and the conversion of aragonite and calcite into hydroxyl apatite (Kasioptas et al., 2008).

Two main processes lead to pseudomorphic (i.e., isovolumetric) mineral replacement. Solid-state reactions are controlled by diffusion; and coupled dissolution re-precipitation (CDR) reactions that are controlled by the solubilities of the parent and product minerals. CDR reactions are common under hydrothermal conditions (Geisler et al., 2005; Xia et al., 2009a). As shown in Fig 1.2, the reaction proceeds via the dissolution of the metastable phase (ABX_2) into the solution of C^+ and D^+ ions and simultaneous re-precipitation of a more stable phase (CDX_2) onto the surface of the parent phase. The reaction proceeds from the surface of the parent phase and then proceeds towards the core, resulting in phase CDX_2 having a high porosity texture. Such porosity is critical for mass transfer between the reaction front and the bulk of the solution (e.g., transport of ions to and from the reaction site), and is essential for CDR reactions (Putnis and Putnis, 2007).

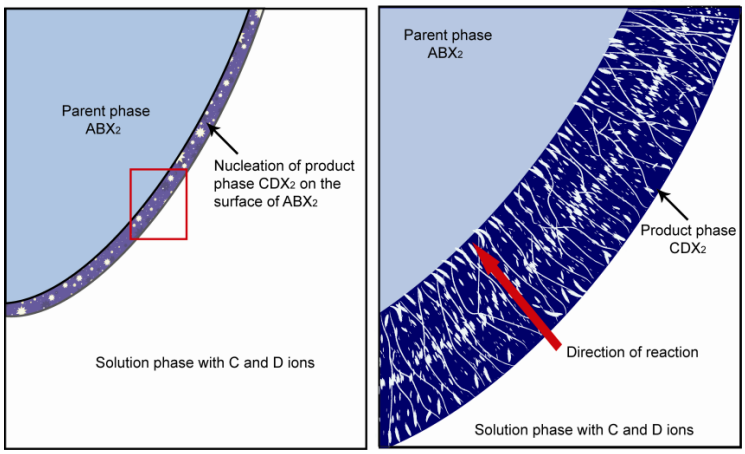

Figure 1.2 Schematic diagram of an interface coupled dissolution-reprecipitation reaction

A pseudomorphic reaction preserves the morphological, and possibly, internal textural features of the parent phase. CDR reactions lead to pseudomorphic replacement when the rate of dissolution of the parent phase is equal to or slower than the rate of precipitation of the product phase at the reaction front (Putnis, 2009). As the reaction advances, the volume of the product precipitated equals the volume of precursor dissolved and precipitation occurs adjacent to the dissolution sites (Putnis, 2002).

The reaction is controlled by the solubility of the parent and product minerals. The kinetics of dissolution and precipitation are controlled by the relative solubilities of the parent and product phase, both of which depend not only on the reaction pressure and temperature, but also on solution compositions (e.g., pH, redox, ligand concentrations). The reaction product may either be a single crystal or polycrystalline, and in some cases information about the crystallographic orientation of the parent mineral is preserved in the product (Xia et al., 2009a).

Based on the studies on transformations achieved by CDR reactions, Putnis (2009) summarized the textural features of these reactions as follows. (1) The product mineral preserves the external dimension and possibly internal textural details of the primary mineral. (2) The product mineral always contains numerous pores and fine cracks. Such porosity is critical in allowing mass transfer between the reaction front and the bulk of the solution (e.g., transportation of ions to and from the reaction site), and is thus essential for CDR reactions (e.g. (Putnis and Putnis, 2007). The generation of porosity depends on two factors: the relative molar volumes of the two solid phases, and the relative solubilities of the two phases in the fluid. (3) There is a sharp reaction front between the parent and product phases.

The unique properties of this reaction mechanism can be applied to a wide range of systems and problems. The study of mineral replacement under hydrothermal conditions develops the understanding of the chemical and physical processes responsible for the formation of hydrothermal ores deposits. At a general level, it will give the information about the physical chemistry of mineral dissolution and crystallization, solution chemistry, and fluid transport through cracks, along grain boundaries and through the porosity generated. Thus, porosity is of paramount importance for enabling efficient fluid/solutes transport and ore deposition.

Further, these reactions can be employed as a new approach in the synthesis of some forms of materials. A recent study by Xia and coworkers reported the synthesis of analcime ($NaAlSi_2O_6 \cdot 3H_2O$) from leucite ($KAlSi_2O_6$) via the hydrothermal pseudomorphic replacement route (Xia et al., 2009b). The resulting analcime presents three-dimensional (3D) ordered arrays of zeolite nanocrystals with uniform size and crystallographic orientation. This type of reaction can also be employed in the mining and processing industries. The hydrothermal mineral replacement reactions from calaverite to native gold has been considered as a promising method for pre-treatment before cyanide leaching for gold extraction from gold telluride ores (Zhao et al., 2010).

Though many mineral replacement reactions have been described over the last few decades, the understanding about mineral replacement reactions are still limited by some complex problems, which are difficult to tackle. For example, we can't predict the scale of porosity and the coupling between porosity and reaction rates.

Porosity in the product mineral is one of the important features of the mineral replacement reactions. However, minerals in nature formed by replacement reactions, such as bornite (Cu_5FeS) in ores are not porous when mined. Putnis et al. (2005) studied the transformation form KBr to KCl and found that the product phase, porous KCl crystal when formed milky was eventually clear after the replacement reaction, and the porosity structure began to disappear within two days at room temperature. However, the processes by which porosity heals (or anneals out) in the product mineral are still difficult to quantify. To gain a better understanding of the closure the porosity structure, the effects on the size, shape, density, and interconnectivity of the pores needs to be studied. This study will develop the knowledge of formation and disappearance of the microstructure in the product mineral and enable more accurate modellings of fluid flow in ore deposit formation with possible applications to predictive exploration and mining.

1.5 Scavenging of Trace and Minor Elements in CDR Reactions

Mineral replacement reactions are prominent in IOCG deposits, such as Olympic Dam and Prominent Hill. Recent studies have demonstrated CDR reactions are part of the paragenesis at Olympic Dam, i.e. the replacement of hematite by chalcopyrite and the replacement of chalcopyrite by bornite (Zhao et al., 2014a; Zhao et al., 2014b), but no specific study on the genesis of U mineralization has been conducted at the deposit.

Tooth et al. (2011) found that Au scavenging occurs during the replacement of pyrrhotite by magnetite in the presence of Bi-melts in hydrothermal fluids. This is a good model system to be used for the study of U in CDR reactions. This phenomenon also exists in natural deposits, like NICO deposit, NWT, Canada (Acosta-Góngora et al., 2015); Stormont skarn prospect, north-western Tasmania (Cockerton and Tomkins, 2012); and the Escanaba

Trough, Southern Gorda Ridge (Törmänen and Koski, 2005). In these systems, infiltrating fluids reduce Bi (III) into elemental Bi-melt (Acosta-Góngora et al., 2015; Tooth et al., 2008; Tooth et al., 2011; Törmänen and Koski, 2005).

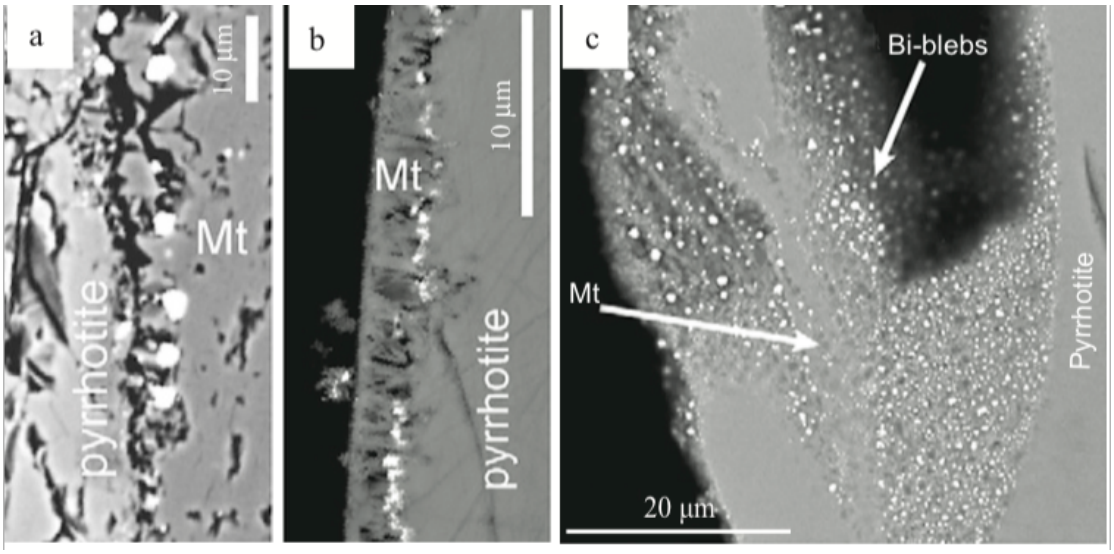

Figure 1.3 (a-c) Bi-blebs forming at the interface during the replacement of pyrrhotite by magnetite (Mt). (a-b) The replacement interface provides appropriate reaction conditions (reducing, low aH_2S, catalytic surfaces) for the formation of Bi-melt that can than scavenge Au from undersaturated hydrothermal fluids. (c) Secondary porosity within the magnetite provides space for the Bi-melt (after Tooth et al. 2011).

In the experimental study, Tooth et al. (2011) recognizes identical textures (Fig. 1.3a, b, c) in the replacement of pyrrhotite by magnetite to show the formation of Bi-melt facilitated by the replacement front, since the Bi melt is stable under reducing conditions and low sulfur activity. Furthermore, the resultant porosity within the magnetite provides space for the Bi-melt (Fig. 1.3c). Those pores also facilitate the scavenging of Au from solution (Altree-Williams et al., 2015).

The natural ore samples collected from Olympic Dam contain fine grained uraninite associated with Cu-Fe sulfides (Fig. 1.4a). Zhao et al. (2014a) reported the replacement of hematite by chalcopyrite under hydrothermal conditions in IOCG deposit (Fig. 1.4b). It is believed that the scavenging of U in IOCG deposit could occur during the transition from

hematite to chalcopyrite. In this thesis, experimental studies were used to investigate the scavenging of uranium during mineral replacement reactions in the Fe-Cu-S hydrothermal system.

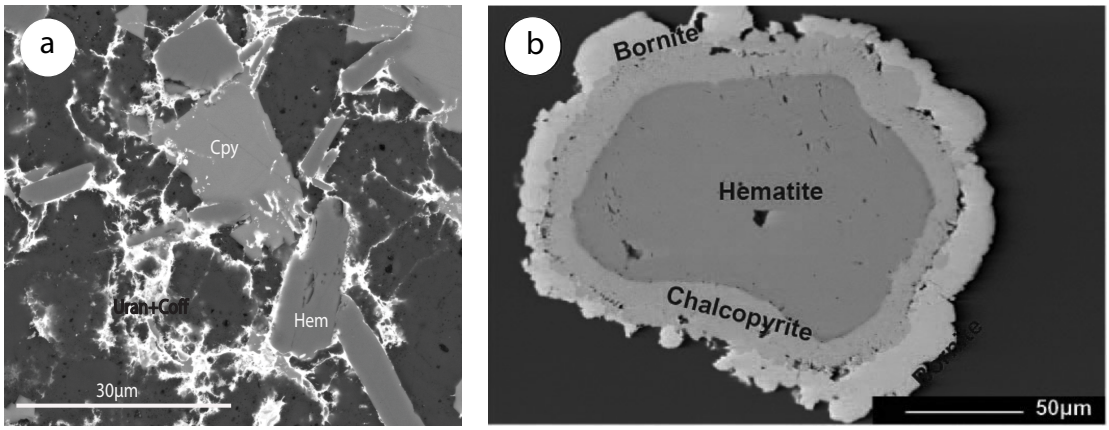

Figure 1.4 (a) SEM image of uranium (uraninite/coffinite) associated with hematite and chalcopyrite from Olympic Dam, South Australia. (b) Cross section of three layered grain, which includes a bornite layer, a chalcopyrite layer and a hematite layer from the mineral replacement reaction starting from hematite (after Zhao et al. 2014a)

1.6 Mineral Replacement Reactions in the Fe-Cu-S system

In the IOCG deposits, the Fe-Cu-S system is important geologically and economically. Table 1.3 lists the general information and physical properties of the dominant minerals associated with Fe in IOCG deposits.

Table 1.3 General information and physical properties of Fe-bearing minerals in IOCG deposits

Mineral	Chemical formula	Color	Density (g/cm^3)	Hard-ness
Chalcopyrite	$CuFeS_2$	Brass yellow, Honey yellow	4.19	3.5
Bornite	Cu_5FeS_4	Copper red, Bronze brown, Purple	4.9-5.3	3
Covellite	CuS	Indigo blue, Light Blue, Dark Blue, Black	4.68	1.5
Chalcocite	Cu_2S	Blue black, Gray, Black, Black gray	5.5-5.8	2.5-3
Digenite	Cu_9S_5	Blue, Dark blue, Black	5.6	2.5-3
Pyrite	FeS_2	Pale brass yellow	5-5.02	6.5
Hematite	Fe_2O_3	Reddish gray, black, blackish red	5.3	6.5
Magnetite	Fe_3O_4	Grayish black, Iron black	5.1-5.2	5.5-6
Note: Data is from http://webmineral .com/data/				

A large number of experimental studies on the Fe-Cu-S system in last few decades were

undertaken using classic dry sealed tube but only a small number under hydrothermal conditions. Fig 1.5 summarizes the phase relations in the central portion of the Fe-Cu-S in the dry conditions. As shown in Figure 1.5a and 1.5b, there are mainly three solid solutions: intermediate solid solution (or chalcopyrite solid solution iss), chalcocite-digenite-bornite(cc-dg-bn) solid solution, and the pyrrhotite solid solution (po) in the phase equilibriums of Fe-Cu-S at 400 ^{o}C and above (Cabri, 1973; Craig and Scott, 1974). The stability of the mineral phases in the Fe-Cu-S system increases as the temperature approaches to 25 ^{o}C (Fig. 1.5c) (Vaughan and Craig, 1978). Furthermore, Kullerud and Yund (1960) indicated the transition from bornite-pyrite into digenite-chalcopyrite at temperature below 228 ^{o}C; and also Cabri (1973) demonstrated that chalcopyrite could break down into an iss + pyrite + vapor at 600 ^{o}C.

Since chalcopyrite and bornite are hydrothermal minerals formed from copper-rich saline fluids in many types of ore deposit, a number of studies on the generation of iron copper sulfide have been undertaken under hydrothermal conditions. Roberts (1961 and 1963) mixed Fe (II) and Cu (II) solutions at low temperature to investigate the nucleation of chalcopyrite and bornite, and pointed out that an iron diffusion process was the mechanism by which Fe-Cu-S minerals were formed. However, the study of Cowper and Rickard (1989) indicated that mixtures of Fe (II), Cu (II) and Na_2S solutions did not result in the nucleation of chalcopyrite; and chalcopyrite could form from the reaction of dissolved of Cu (II) salts with natural hexagonal pyrrhotite ($Fe_{0.9}S$). They also provided the evidence from the reactions between pyrite and Cu (II) to show that the reaction rate could be controlled by the concentration of Cu (II) (Rickard and Cowper, 1994). Chalcopyrite also was synthesized by Hu et al. (1999) by dissolving CuCl (s), $FeCl_3 \cdot H_2O$ (s) and $(NH_4)_2S$ (s) in aqueous solution in autoclaves up to 250 ^{o}C for 3 hours. A similar method also was employed to make

chalcopyrite nanowires by Wang et al. (2009).

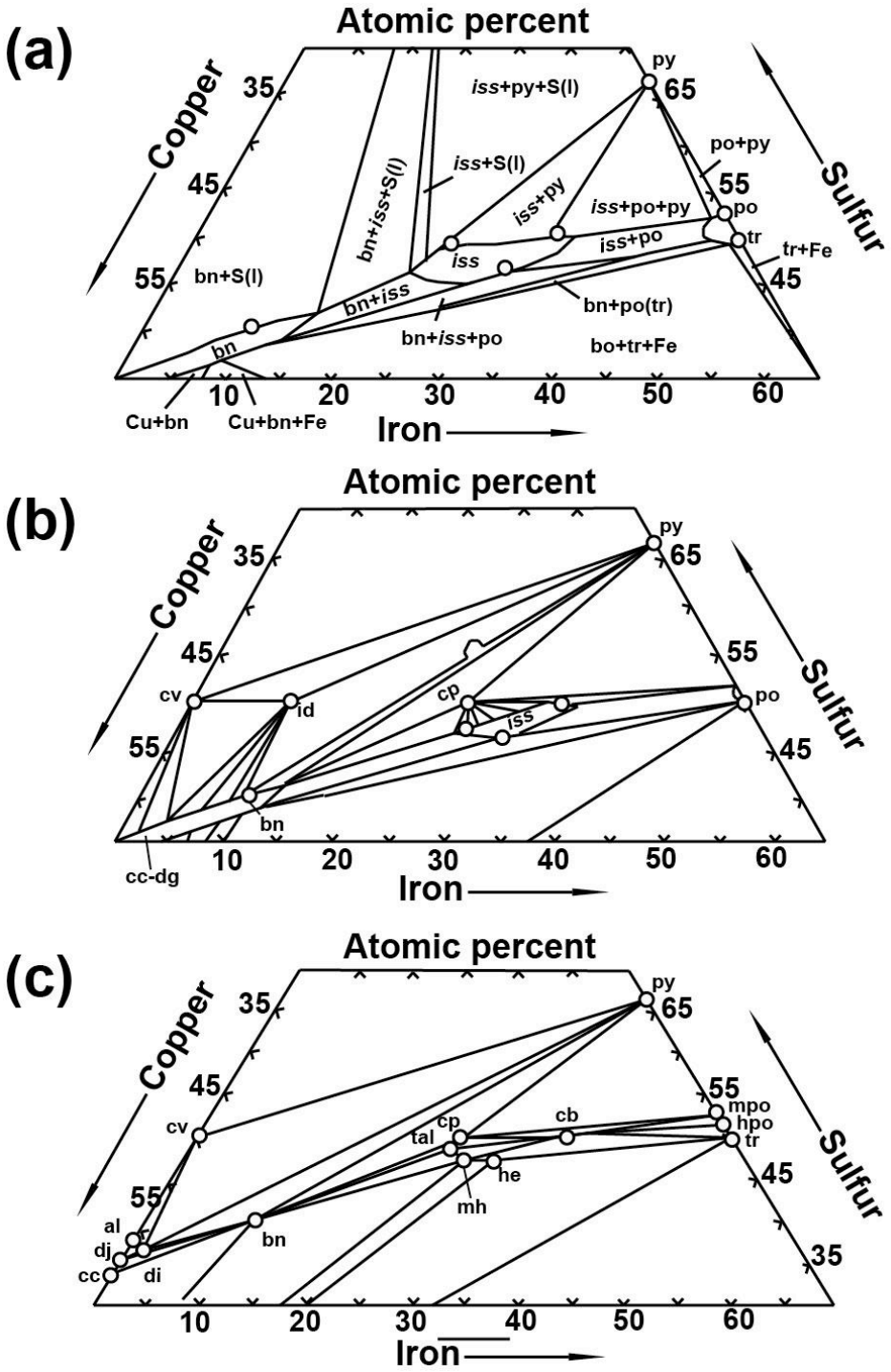

Figure 1.5 Phase relations in the central portion of the Fe-Cu-S sytem (a) at 600 ºC (after Cabri 1973); (b) at 400 ºC (after Craig and Scott 1974); (c) at 25 ºC (after Vaughan and Craig 1978)

The methods above of chalcopyrite formation under hydrothermal conditions do not mimic

the real conditions in nature. Recently, Zhao et al. (2014a) produced chalcopyrite and bornite hydrothermally via mineral replacement reactions (Fig. 1.4b). Hematite, as starting material, could be replaced by chalcopyrite in Cu (I) and hydrosulfide solutions heated up to 300 ^{o}C at vapor-saturated pressures. This outcome matches the report of chalcopyrite replacing hematite from numerous different ore-forming environments, such as Kupferschiefer type deposits (Kucha and Pawlikowski, 1986) and IOCG deposits (Kiruna type) (Edfelt et al., 2005). With the continuing replacement, bornite was observed to replace the earlier-formed chalcopyrite phase, which has also been observed in natural ores from Indian Ocean hydrothermal veins (Halbach et al., 1998).

1.7 Research Objectives

The principal objective of this research is to understand uranium scavenging from hydrothermal fluids during ICDR reactions, thus helping to elucidate the Cu-U association in IOCG deposits. To achieve this aim, two sets of experimental studies on U-scavenging in Fe-Cu-S system were designed and presented in this thesis. In Chapter 3, uranium precipitation from different uranium sources during the mineral replacement reaction of hematite by chalcopyrite will be presented. This replacement model was recently studied by Zhao et al. (2014a). In Chapter 4, the experimental replacement among chalcopyrite, bornite and digentite to study U-scavenging with the different experimental conditions will be examined. Those two experimental studies could help to understand the processes that scavenge U during fluid-rock interaction and the potential effect of ICDR reactions in promoting/inhibiting metal recovery during ore leaching. These two chapters also describe the occurrence of U-bearing minerals with hematite, chalcopyrite and bornite in ores from IOCG deposits, like Olympic Dam and Moonta Mines. Textural observations on natural ores were used to determine the deportment of uranium in relation to the replacement of

hematite by chalcopyrite, chalcopyrite by bornite, and bornite by chalcopyrite. Comparisons between natural ores and experimental analogues assists in understanding the paragenetic position of uraninite and other uranium minerals in these IOCG ores, which is important for efficient extraction of uranium and its decay products from Cu concentrates.

In order to decipher the mechanism of uranium scavenging in nature ores, it is essential to understand the distribution and speciation of uranium and other dominant elements. Chapter 5 introduces the application of Megapixel-synchrotron X-ray fluorescence (MSXRF) on thin-section scale element mapping at μm-scale spatial resolution and ppm-level detection limits. The MSXRF elements maps obtained from different types of U deposit, like IOCG and sediment-hosted U, provided the evidence to show the formation of U-bearing minerals under various conditions. Therefore, this chapter also covers the investigation on other minor elements from different geological contexts, such as Pt in PGE deposits and Ge in vein-type polymetallic hydrothermal deposit utilising the MSXRF mapping technique.

In Chapter 6, the overall investigations and findings of this thesis will be summarized and some possible suggestions on future work will be listed. The author's other publications related to this research are attached in the Appendix at the end of this thesis.

1.8 References

Acosta-Góngora, P., Gleeson, S., Samson, I., Ootes, L., and Corriveau, L., 2015, Gold Refining by Bismuth Melts in the Iron Oxide-Dominated NICO Au-Co-Bi (±Cu±W) Deposit, NWT, Canada: Economic Geology, v. 110, p. 291-314.

Altree-Williams, A., Pring, A., Ngothai, Y., and Brugger, J., 2015, Textural and compositional complexities resulting from coupled dissolution-reprecipitation reactions in geomaterials: Earth-Science Reviews, v. 150, 628-651.

Association, W. N., 2014, Australia's uranium, 2015.

BHP Billiton, 2011, Olympic Dam Expansion: Supplementary Environmental Impact Statement, 2011, BHP Billiton.

Birch, G., Every, C., Märten, H., Marsland-Smith, A., Phillips, R., and Woods, P., 2013, Beverley uranium mines, heathgate resources: Australasian Mining and Metallurgical Operating Practices,(Australasian Inst. Min. Metall., Melbourne, Australia), v. 2, p. 1799-1818.

Cabri, L. J., 1973, New data on phase relations in the Cu-Fe-S system: Economic Geology, v. 68, p. 443-454.

Ceyhan, M., 2009, World distribution of uranium deposits (UDEPO) with uranium deposit classification: IAEATECDOC-1629, Division of Nuclear Fuel Cycle.

Cockerton, A. B., and Tomkins, A. G., 2012, Insights into the Liquid Bismuth Collector Model Through Analysis of the Bi-Au Stormont Skarn Prospect, Northwest Tasmania: Economic Geology, v. 107, p. 667-682.

Cowper, M., and Rickard, D., 1989, Mechanism of chalcopyrite formation from iron monosulphides in aqueous solutions (< 100° C, pH 2–4.5): Chemical geology, v. 78, p. 325-341.

Craig, J., and Scott, S., 1974, Sulfide phase equilibria: Sulfide mineralogy, v. 1, p. CS1-110.

Edfelt, Å., Armstrong, R. N., Smith, M., and Martinsson, O., 2005, Alteration paragenesis and mineral chemistry of the Tjårrojåkka apatite–iron and Cu (-Au) occurrences, Kiruna area, northern Sweden: Mineralium Deposita, v. 40, p. 409-434.

Geisler, T., Seydoux-Guillaume, A.-M., Poeml, P., Golla-Schindler, U., Berndt, J., Wirth, R., Pollok, K., Janssen, A., and Putnis, A., 2005, Experimental hydrothermal alteration of crystalline and radiation-damaged pyrochlore: Journal of nuclear materials, v. 344, p. 17-23.

Halbach, P., Blum, N., Münch, U., Plüger, W., Garbe-Schönberg, D., and Zimmer, M., 1998, Formation and decay of a modern massive sulfide deposit in the Indian Ocean: Mineralium Deposita, v. 33, p. 302-309.

Hu, J., Lu, Q., Deng, B., Tang, K., Qian, Y., Li, Y., Zhou, G., and Liu, X., 1999, A hydrothermal reaction to synthesize CuFeS 2 nanorods: Inorganic Chemistry Communications, v. 2, p. 569-571.

Idnurm, M., and Heinrich, C., 1993, A palaeomagnetic study of hydrothermal activity and uranium mineralization at Mt Painter, South Australia: Australian Journal of Earth Sciences, v. 40, p. 87-101.

Jaireth, S., Clarke, J., and Cross, A., 2010, Exploring for sandstone-hosted uranium deposits in paleovalleys and paleochannels: AusGeo News, v. 97, p. 21-25.

Kasioptas, A., Perdikouri, C., Putnis, C., and Putnis, A., 2008, Pseudomorphic replacement of single calcium carbonate crystals by polycrystalline apatite: Mineralogical Magazine, v. 72, p. 77-80.

Kucha, H., and Pawlikowski, M., 1986, Two-brine model of the genesis of strata-bound Zechstein deposits (Kupferschiefer type), Poland: Mineralium Deposita, v. 21, p. 70-80.

Kullerud, G., and Yund, R., 1960, The Cu—S system: Geological Society of America Bulletin, v. 71, p. 1911-12.

McKay, A. D., and Miezitis, Y., 2001, Australia's uranium resources, geology and development of deposits, AGSO-Geoscience Australia.

Mudd, G. M., 2008, Radon releases from Australian uranium mining and milling projects: assessing the UNSCEAR approach: Journal of environmental radioactivity, v. 99, p. 288-315.

Putnis, A., 2002, Mineral replacement reactions: from macroscopic observations to microscopic mechanisms: Mineralogical Magazine, v. 66, p. 689-708.

Putnis, A., 2009, Mineral replacement reactions: Reviews in mineralogy and geochemistry, v. 70, p. 87-124.

Putnis, A., and Putnis, C. V., 2007, The mechanism of reequilibration of solids in the presence of a fluid phase: Journal of Solid State Chemistry, v. 180, p. 1783-1786.

Putnis, C. V., and Mezger, K., 2004, A mechanism of mineral replacement: isotope tracing in the model system KCl-KBr-H 2 O: Geochimica et Cosmochimica Acta, v. 68, p. 2839-2848.

Putnis, C. V., Geisler, T., Schmid-Beurmann, P., Stephan, T., and Giampaolo, C., 2007, An experimental study of the replacement of leucite by analcime: American Mineralogist, v. 92, p. 19-26.

Putnis, C. V., Tsukamoto, K., and Nishimura, Y., 2005, Letter. Direct observations of pseudomorphism: compositional and textural evolution at a fluid-solid interface: American Mineralogist, v. 90, p. 1909-1912.

Rickard, D., and Cowper, M., 1994, Kinetics and mechanism of chalcopyrite formation from Fe (II) disulphide in aqueous solution (< 200° C): Geochimica et cosmochimica acta, v. 58, p. 3795-3802.

Roberts, W., 1961, Formation of chalcopyrite by reaction between chalcocite and pyrrhotite in cold solution: Nature, v. 191, p. 560-562.

Roberts, W., 1963, The low temperature synthesis in aqueous solution of chalcopyrite and bornite: Economic Geology, v. 58, p. 52-61.

Taylor, G., Farrington, V., Woods, P., Ring, R., and Molloy, R., 2004, Review of environmental impacts of the acid in-situ leach uranium mining process, CSIRO Land and Water Client Report, CSIRO Clayton, Victoria, p. 60.

Tooth, B., Brugger, J., Ciobanu, C., and Liu, W., 2008, Modeling of gold scavenging by bismuth melts coexisting with hydrothermal fluids: Geology, v. 36, p. 815-818.

Tooth, B., Ciobanu, C. L., Green, L., O'Neill, B., and Brugger, J., 2011, Bi-melt formation and gold scavenging from hydrothermal fluids: An experimental study: Geochimica et Cosmochimica Acta, v. 75, p. 5423-5443.

Törmänen, T. O., and Koski, R. A., 2005, Gold enrichment and the Bi-Au association in pyrrhotite-rich massive sulfide deposits, Escanaba Trough, Southern Gorda Ridge: Economic Geology, v. 100, p. 1135-1150.

Vaughan, D. J., and Craig, J. R., 1978, Mineral chemistry of metal sulfides, Cambridge University Press.

Wang, M., Wang, L., Yue, G., Wang, X., Yan, P., and Peng, D., 2009, Single crystal of CuFeS 2 nanowires synthesized through solventothermal process: Materials Chemistry and Physics, v. 115, p. 147-150.

Weisheit, A., Bons, P. D., and Elburg, M. A., 2013, Long-lived crustal-scale fluid flow: the hydrothermal mega-breccia of Hidden Valley, Mt. Painter Inlier, South Australia: International Journal of Earth Sciences, v. 102, p. 1219-1236.

Xia, F., Brugger, J., Chen, G., Ngothai, Y., O'Neill, B., Putnis, A., and Pring, A., 2009a, Mechanism and kinetics of pseudomorphic mineral replacement reactions: a case study of the replacement of pentlandite by violarite: Geochimica et Cosmochimica Acta, v. 73, p. 1945-1969.

Xia, F., Brugger, J., Ngothai, Y., O'Neill, B., Chen, G., and Pring, A., 2009b, Three-Dimensional Ordered Arrays of Zeolite Nanocrystals with Uniform Size and Orientation by a Pseudomorphic Coupled Dissolution− Reprecipitation Replacement Route: Crystal Growth & Design, v. 9, p. 4902-4906.

Zhao, J., Brugger, J., Chen, G., Ngothai, Y., and Pring, A., 2014a, Experimental study of the formation of chalcopyrite and bornite via the sulfidation of hematite: Mineral replacements with a large volume increase: American Mineralogist, v. 99, p. 343-354.

Zhao, J., Brugger, J., Ngothai, Y., and Pring, A., 2014b, The replacement of chalcopyrite by bornite under hydrothermal conditions: American Mineralogist, v. 99, p. 2389-2397.

Zhao, J., Xia, F., Pring, A., Brugger, J., Grundler, P. V., and Chen, G., 2010, A novel pre-treatment of calaverite by hydrothermal mineral replacement reactions: Minerals Engineering, v. 23, p. 451-453.

Chapter 2

Research Methodology

This chapter covers the details of the natural and synthetic starting materials, buffer solution preparation, hydrothermal experiments, and all of the analytical methods utilized in these studies. These analytical techniques include powder X-ray diffraction (XRD), field emission scanning electron microscopy (FESEM), focussed ion beam scanning electron microscopy (FIB-SEM), transmission electron microscopy (TEM), electron probe microanalysis (EPMA), X-ray absorption near edge structure (XANES) spectra analysis, and megapixel-synchrotron X-ray fluorescence (MSXRF) mapping.

2.1 Natural samples

In the studies covered by this thesis, two natural minerals were used as starting material in the hydrothermal reactions: micaceous hematite from Cumberland, England (SA Museum No G6983) and chalcopyrite from Moonta mine, South Australia, Australia (SA Museum G22621). The compositions of the two minerals are given in Table 2.1 as determined by EPMA. Both the hematite and the chalcopyrite natural samples were crushed and sieved into 125 – 150 μm fractions; and washed in the ultrasonic bath before use in hydrothermal experiments.

In addition, samples from four different mining districts were studied. They were made into thin-sections for investigating both major and minor components. Three high-grade samples collected from pre-mining cores from the Beverley North mine area of Lake Frome Embayment, Northern Flinders Ranges, South Australia. One sample was collected from Pannikan (bore-hole number PRC021 at 260.4 m depth, labelled Bev21.6), and other two samples from Pepegoona (bore-holes PRC013 at 200.3 m depth, and PRC015 at 219.2 m depths, labelled Bev13.1 and Bev15.3, respectively). Since samples from Beverley are

poorly consolidated sediments, they were embedded in epoxy resin, glued onto 1 mm quartz slides, and polished under oil to a thickness of ~100 μm.

Table 2.1 Composition of starting materials

Hematite (Cumberland, England, SA Museum G6983) (Analysis on 21 Points)(wt%)			
	Mean	**Range**	**Standard deviation**
Fe_2O_3	97.33	94.35-100.69	0.36
SiO_2	1.21	<0.06-2.98	0.06
Al_2O_3	0.05	<0.06-0.17	0.06
MgO	0.04	<0.05-0.10	0.05
MnO_2	0.03	<0.06-0.08	0.06
P_2O_5	0.04	<0.05-0.13	0.05
Total	**98.53**		
Chalcopyrite (Moonta Mines, Australia, SA Museum G22621) (Analysis on 24 Points)(wt%)			
	Mean	**Range**	**Standard deviation**
Cu	35.46	35.21-35.77	0.29
Fe	31.23	31.02-31.35	0.29
S	33.49	33.23-33.81	0.25
Total	**98.53**		

In order to decipher the nature and origin of the U mineralisation at Moonta mines, two bornite-rich ore samples from Moonta (SA Museum G555 and G7646a) were selected based on a radiometric survey of eight historic samples within the SA Museum collection. In the study on ore petrography using megapixel X-ray imaging, samples from Barrigão deposit, Alentejo Province, Portugal and Fifield Pt-Au field, New South Wales, Australia were selected to investigate the distribution of Pt, Ge, and As. Standard polished thin sections (30 μm), mounted on 1 mm thick quartz glass slides, were prepared for the samples from Moonta and Barrigão. The other sample from Fifield was embedded in epoxy resin and the block of size of 4 x 2 x 2 cm (length x width x thickness) and polished (1 μm diamond paste).

2.2 Synthesis of uraninite

Synthetic uraninite was used as a U^{4+} source for the hydrothermal experiments. It was produced by the reduction of high purity $UO_2(NO_3)_2$ by Zn metal as follows: $UO_2(NO_3)_2$ was dissolved in 1 M HCl; O_2(aq) was removed by bubbling a 99.5% N_2 and 0.5% H_2 gas mixture through the solution, which was then sealed into Teflon-lined autoclaves. The autoclaves were kept at 150 ^oC for 3 days. After cooling, the products were washed in 10 M HCl several times until no further bubbles were released in order to remove Zn and U(VI) impurities. Finally, the products were washed in Milli-Q water (resistance of 18 MΩ cm^{-1}, Direct-Q3 system, Millipore Corp) and acetone. The synthetic uraninite has a unit cell size *a* = 5.4105(2) Å (V = 158.38(2) $Å^3$), as refined using TOPAS (Bruker, 2005). This unit cell dimension is typical for uraninite found in hydrothermal environments (Fritsche and Dahlkamp, 1997), and corresponds to a uraninite composition $UO_{2.56}$ (Grønvold, 1955; Singh et al., 2011).

2.3 Preparation of buffer solution

Acetate buffer solutions ranging from pH 4-6 were employed in experimental studies. Mill-Q water was used to prepare buffer solution at room temperature. A temperature-corrected pH-meter (EUTECH Scientific, model Cyber-scan 510) with an Ag/AgCl pH electrode was used for the pH measurements. Thioacetamide (CH_3CSNH_2) was used for providing S in the experiments. Thioacetamide is stable at room temperature, but above 100 ^oC, it decomposes and releases H_2S, which acts to buffer the original solution. The HCh thermodynamic equilibrium program (Shavarov, 1999) was used to calculate the buffer pH at 25 ^oC and 300 ^oC with 0.025 moles thioacetamide. The composition of the buffer solutions and calculated pH values are list in Table 2.2. To prevent disproportionation of Cu(I) complexes, 1 molal NaCl was added to the solution (Brugger et al., 2007).

Table 2.2 Composition of buffer solutions and calculated pH from HCh

No.	Component	Cal	pH without S		pH With S		Addition
		25 °C	25 °C	300 °C	25 °C	300 °C	NaCl
C4	0.83 m CH_3COOH + 0.17 m CH_3COONa	3.98	3.76	4.51	3.7	4.52	1 molar
C5	0.30 m CH_3COOH + 0.70 m CH_3COONa	5.03	4.76	5.39	4.75	5.37	1 molar
C6	0.06 m CH_3COOH + 0.96 m CH_3COONa	6.14	5.60	6.19	5.49	5.88	1 molar

2.4 Hydrothermal experiments

In order to investigate the scavenging of U in Cu-Fe-S minerals, three sets of hydrothermal experiments with hematite and chalcopyrite as starting materials respectively, were performed via the *in situ* hydrothermal method. 25 ml polytetrafluoroethylene (PTFE) cells sealed in stainless steel static batch reactors (Fig. 2.1) were used to undertake the experiments up to 220 °C. Other experiments were carried out using 8 ml titanium autoclaves (Fig. 2.2). All of starting materials were loaded into reactors in the N_2-filled anoxic glove box to avoid O_2 joining the reactions.

Electric muffle furnaces or ovens (Fig 2.3) (both with a temperature regulation precision of ±2°C) were used to heat the hydrothermal reactors at a constant temperature for the duration of experiments. During the experiments, the pressures in the autoclaves reach autogenesis vapor pressure. After reactions, the autoclaves were quenched in a large volume (~10 l) of cold water for 45 minutes. The reacted fluid was collected, and solid were rinsed three times with Milli-Q water and then once with acetone before drying.

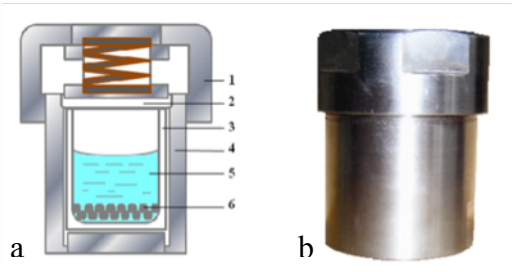

Figure 2.1 Schematic diagram (a) and picture (b) of PTFE lined stainless steel static batch reactors. In the schematic diagram: 1 stainless steel cap, 2 PTFE cap, 3 PTFE body, 4 stainless steel body, 5 hydrothermal reaction fluid, 6 mineral samples

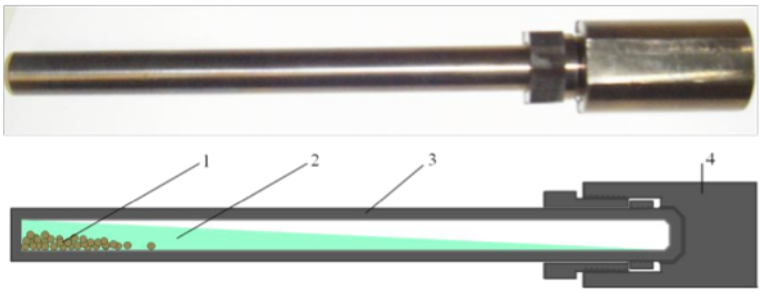

Figure 2.2 Titanium autoclave reactor (above photograph, below diagram). 1 Mineral grains, 2 reaction solution, 3 reactor body, 4 titanium cap

Figure 2.3 ovens (a) and Muffle furnaces (b) used in this work. These furnaces/ovens are programmable and the temperature can be controlled precisely with ±2 ^{o}C. The maximum working temperature of the furnaces and ovens are 1150 ^{o}C and 500 ^{o}C, respectively.

2.5 Powder X-ray diffraction (XRD)

Mineral phases in natural and experimental samples were identified and quantified by powder X-ray diffraction (XRD), a standard technique for inorganic materials phase identification and quantification. The basic principle of XRD is according to the classic Bragg's law:

$\lambda = 2d \sin\theta$

where λ is the wavelength of X-ray, d is the distance between sets of crystal hkl planes, and θ is the diffraction angle. Mineral phases can be identified and subsequently quantified via comparing the obtained pattern with standard patterns from databases. Pecharsky and Zavalij (2003) provided further details about XRD principles.

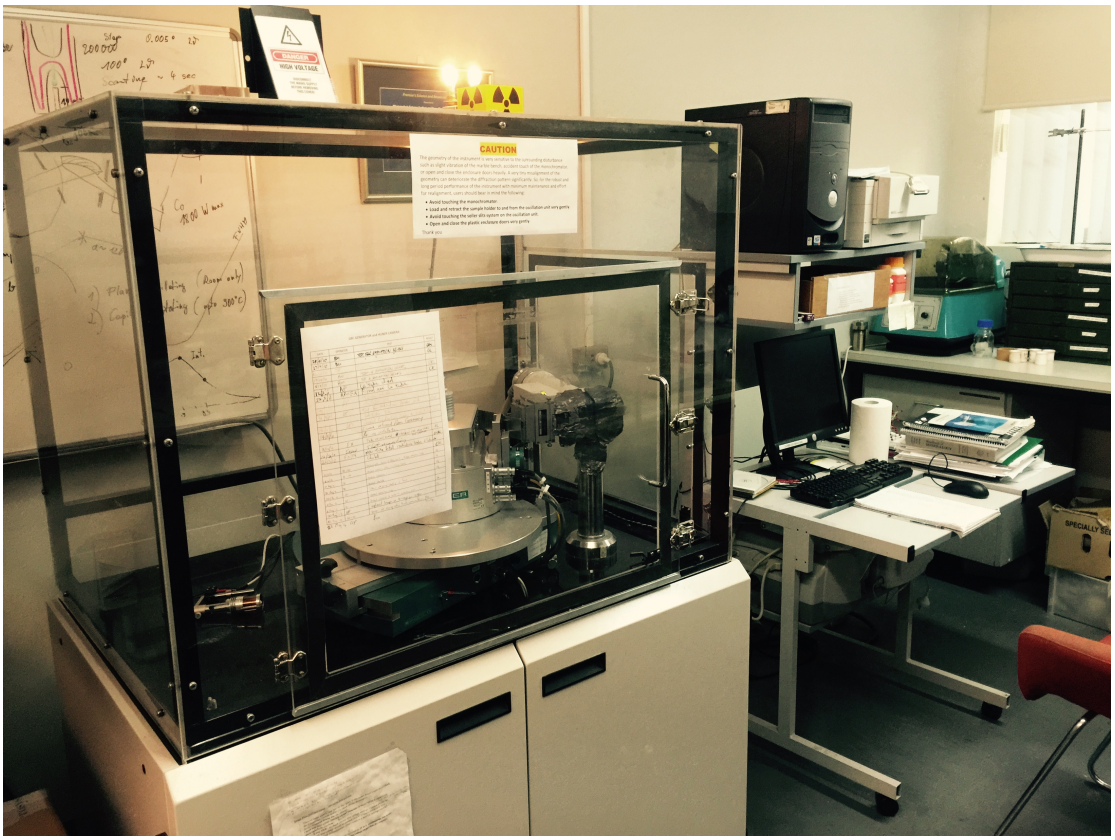

Figure 2.4 The Huber Guinier Imaging Plate Camera G670

XRD patterns were collected on a Huber Guinier Imaging Plate Camera G670 with CoKα_1 radiation (λ=1.78892 Å) (Fig. 2.4) at Mineralogy Department, SA Museum. The X-ray was generated by a PANalytical® X-ray tube at 35 kV and 34 mA, and filtered by an asymmetrically ground and curved quartz (SiO_2) monochromator. The function of the HUBER Imaging Plate Camera is based on the image properties of a 330 x 15 mm X-Ray sensitive storage film, which is arranged in a focal circle 180 mm in diameter. A laser scanner reads the image information of the diffraction pattern on the film. A focused laser beam (30 x 50 μm) excites photoluminescence on the film which is detected by a photomultiplier. The obtained signal is amplified, digitized by an A/D-converter and transferred to the memory of the controlling computer. The image plate records diffraction patterns with 2θ range from 4° to 100° with a step of 0.005°. Approximately 5 mg of grounded sample was spread on a MYLAR® polyethylene terephthalate thin film for each XRD analysis. Quantitative phase analysis (QPA) of each sample was determined with the program Topas (Bruker, 2005). The analysis was normalised to 100 wt%; Note that bulk powder diffraction cannot detect phases below ~3 wt%, and amorphous or poorly crystalline phases are not readily quantifiable.

2.6 Scanning electron microscopy (SEM)

A scanning electron microscope (SEM) is a type of electron microscope that produces images of a sample by scanning it with a focused beam of electrons. It is an important instrument for the examination and analysis of the microstructure characteristics of solid objects. Various signals produced from the interaction between atoms in the sample and the electron beam can be detected providing information about the sample's surface topography and composition (Goldstein et al., 2012). Secondary electron (SE) is the most common imaging mode, in which electrons are ejected from the k-shell of the specimen atoms by

inelastic scattering interactions with beam electrons. Due to their low energy, these electrons originate from within a few nanometers of the sample surface (Goldstein et al., 2012). Backscattered electrons (BSE) consist of high-energy electrons originating from the electron beam, which are reflected out of the specimen interaction volume by elastic scattering interactions with specimen atoms. Heavy elements (high atomic number) provide stronger backscatter electrons than lighter elements (low atomic number); thus heavy elements appear brighter in images. BSE is helpful for the determination of the sample chemical composition (Goldstein et al., 2012).

Figure 2.5a Philips XL30 field emission scanning electron microscope

Figure 2.5b FEI Quanta 450 FEG environmental scanning electron microscopy

A Philips XL30 field emission scanning electron microscope (FESEM) (Fig. 2.5a) and a FEI Quanta 450 FEG environmental scanning electron microscopy (ESEM) (Fig. 2.5b) were employed for scanning electron microscopic analyses at Adelaide Microscopy, University of Adelaide. Both microscopes are equipped with secondary electron (SE) detectors, backscattered electron (BSE) detectors and EDAX® Energy Dispersive X-ray Spectrometers (EDS). The SE detector was used to determine the surface morphology of the grains; and BSE mode could help to characterize the chemical features. For textural investigations, mineral grains were embedded into epoxy resin blocks and polished down to 1 μm, and coated with 15 nm thick carbon films.

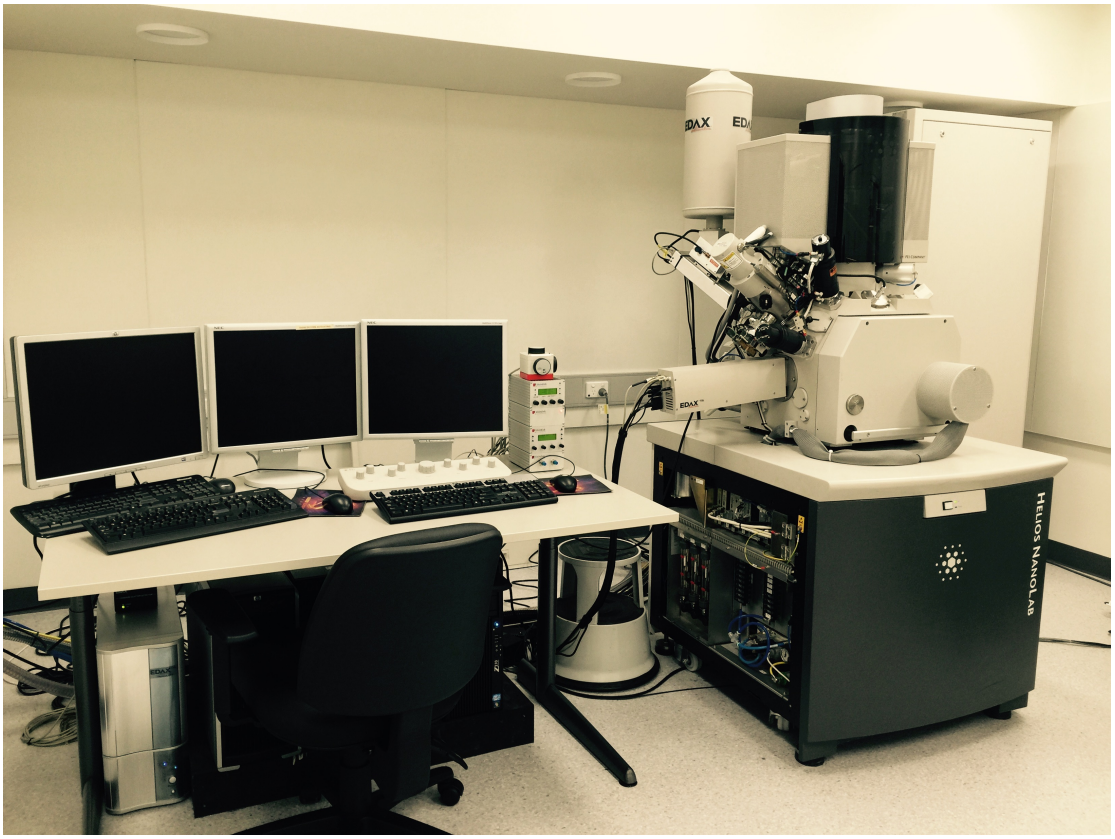

Figure 2.6 FEI Helios 600 Nanolab DualBeam™ Focused Iron Beam FIB/SEM platform

A FEI Helios 600 Nanolab DualBeam™ Focused Iron Beam FIB/SEM platform (Fig. 2.6) at Adelaide Microscopy, University of Adelaide was used to obtain high-resolution SEM images of sample surfaces down to the nanoscale, prepare cuts and extract thin sections (10 x 10 x 5 μm^3) from well-controlled areas within the sample. Ablation was preformed using a Ga beam (20-30 kV/0.093-0.21 nA). Chemical maps were also obtained using the instrument's EDS system.

2.7 Transmission electron microscopy (TEM)

The technique of transmission electron microscopy (TEM) provides a beam of electrons, which is transmitted through an ultra-thin specimen, and interacts with the specimen as it passes through. The information obtained from the interaction of the electrons is used to

form the TEM image. Images produced by TEM come with a significantly higher resolution than light microscopes, because of the small de Broglie wavelength of electrons. This technique is widely used to determine fine detail-even as small as a single column of atoms (Reimer, 2013).

Figure 2.7 FEI Tecnai G2 Spirit TEM

High-resolution images for nanoscale U particles in experimental grains were obtained using TEM. A FEI Tecnai G2 Spirit TEM (Fig. 2.7) located in Adelaide Microscopy, University of Adelaide, was used for imaging, which is equipped with a FEG LaB6 emitter and BiotTWIN lens design, and operated at voltages of 20-120 kV. Imaging was done via an in-column Olympus-SIS Veleta CCD camera. The EDS system helped to characterize chemical features on nano-particles. All of TEM samples were prepared under a FEI Helios 600 Nanolab DualBeam^{TM} Focused Iron Beam FIB/SEM platform.

2.8 Chemical analysis of solid products

Electron probe microanalysis (EPMA), frequently referred to as the electron microprobe, is an analytical tool used to determine the chemical composition of solid materials (Wittry, 1958). It is similar to SEM in that the sample is bombarded with an electron beam, emitting X-rays characteristic to the elements being analysed, which can yield both qualitative and quantitative compositional information of small region (~μm) from a specimen (Goldstein et al., 2012). This technique is widely used in mineralogy to measure the change in elemental composition in mineral samples, which can yield information about the history of the evolution of a crystal, including the temperature, pressure, and chemistry of the surrounding medium (Sweatman and Long, 1969).

Figure 2.8 The CAMECA SX51 electron microprobe

A Cameca SX-51 electron microprobe at Adelaide Microscopy, University of Adelaide (Fig. 2.8) was used to investigate the chemical composition and element distribution of the

starting minerals. The EPMA was equipped with four wavelength dispersive X-ray Spectrometers (WDS), one EDS and one reflected-light optical microscope. Samples for analysis by EPMA were polished with diamond paste (3 and 1 μm) for 20 minutes before being coated with a carbon film. EPMA was operated at an accelerating voltage of 20 kV and a beam current of ~20 nA. The counting time for each element was set at 30 seconds.

2.9 X-ray absorption near edge structure spectra (XANES) analysis

X-ray absorption near edge structure spectra analysis (XANES) can be used to determine the speciation and oxidation state of trace elements in minerals *in-situ* with μm-scale spatial resolution (Brugger et al., 2008; Brugger et al., 2010). Thus, this technique was employed to identify the oxidation state of U in the reacted grains in order to understand the reaction mechanism.

Uranium L_{III}-edge X-ray absorption near edge structure (XANES) spectra were collected at beamline I18 at the Diamond Light Source, Oxfordshire, UK. I18 is an undulator beam line with a Si(111) double crystal monochromator; at 17 keV the energy resolution was ~2.4 eV (1.4×10^{-4}) and the flux ~10^{10} photons/s. The beam was focused to a size of ~6 x 2.2 μm^2 using Kirkpatrick-Baez (KB) mirrors, and fluorescence data was collected with a 9 element Ge detector. The energy was calibrated using a Y foil (first derivative maximum at 17,038 eV for the Y K- edge). The average oxidation state of U can be retrieved from the U L_{III}-edge XANES spectra by measuring the position of the white line that shifts by 3.75–4.3 eV from U^{4+} to U^{6+} (Bertsch et al., 1994; Yamamoto et al., 2008), or the presence of a band at around 17,232 eV related to uranyl resonance (Conradson, 1998). For this study it was sufficient to compare the XANES spectra of experimental samples with those of two U

mineral standards: saleeite, $(Mg(U^{6+}O_2)(PO_4)_2 \bullet 10H_2O$, Ranger Mine, Northern Territory, Australia, Museum Victoria Sample M41723; and cleusonite, Pb $(U^{4+}, U^{6+})(Ti,Fe^{2+},Fe^{3+})_{20} \bullet (H_2O)_{38}$, Cleuson, Valais, Switzerland, (Wülser et al., 2005), South Australian Museum sample G29393. Saleeite contains U^{6+} as a uranyl ion UO_2^{2+}; and cleusonite is nominally a U^{4+} mineral, although it may contain small amounts of U^{6+}/U^{5+} due to radiation damage and weathering. XANES spectra were measured on a FIB slice cut from the sample.

2.10 Megapixel synchrotron X-ray fluorescence mapping and data analysis

The major and minor elements in our natural samples were mapped using the Maia detector array (Fig. 2.9a) developed by CSIRO and Brookhaven National Laboratory (Kirkham et al., 2010; Ryan et al., 2010; Ryan et al., 2014) installed at the XFM beamline (Fig.2.9b), Australian Synchrotron, Melbourne, Australia (Paterson et al., 2011). The beam energy was set at 18.5 keV, and the beam focused to a ~2 µm spot size using KB mirrors. Standard foils (Pt, Mn, Fe) were used to constrain (i) detector efficiency and geometry (e.g., distance from the sample), (ii) any filters that are used in front of the detector; and to (iii) convert from ion chamber counts to flux (photons/sec) (Ryan et al., 2010). The area of each sample was mapped using different scanning speeds (4.1 to 7 mm/s), corresponding to dwell times of 0.49 to 1.22 ms/pixel; the parameters were selected depending on the size of the area to be mapped and the beam time available.

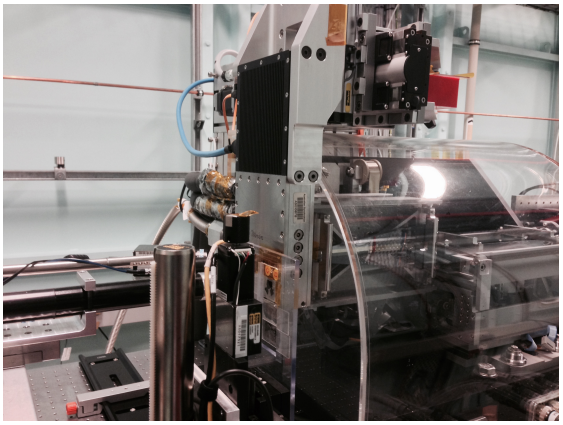

Figure 2.9a Maia detector

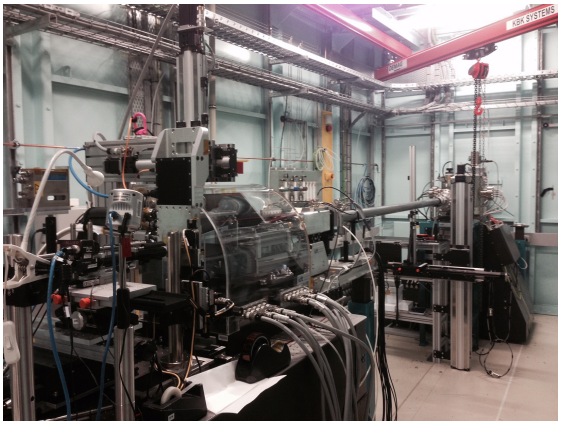

Figure 2.9b XFM beamline in Australian Synchrotron

The MSXRF data were analysed with GeoPIXE (Ryan et al., 2005), using the dynamic analysis (DA) method to project quantitative elemental images from the full fluorescence spectra (Ryan et al., 2010; Ryan et al., 2009; Ryan et al., 2005). The DA technique is a matrix transform algorithm that unfolds overlaps (considering all involved X-ray lines) and subtracts background, escape peaks, and other detector artefacts. By fitting all the available X-ray emission lines for each element present in the sample, the method benefits from better counting statistics than algorithms based on regions of interest (ROIs), and makes it possible to distinguish between elements that have overlapping X-ray lines, which are traditionally difficult to separate using ROIs, e.g. $AuL_{\alpha 1}$ and $ZnK_{\beta 1}$.

2.11 References

Bertsch, P. M., Hunter, D. B., Sutton, S. R., Bajt, S., and Rivers, M. L., 1994, In situ chemical speciation of uranium in soils and sediments by micro X-ray absorption spectroscopy: Environmental science & technology, v. 28, p. 980-984.

Brugger, J., Etschmann, B., Liu, W., Testemale, D., Hazemann, J.-L., Emerich, H., Van Beek, W., and Proux, O., 2007, An XAS study of the structure and thermodynamics of Cu (I) chloride complexes in brines up to high temperature (400 C, 600bar): Geochimica et Cosmochimica Acta, v. 71, p. 4920-4941.

Brugger, J., Etschmann, B., Pownceby, M., Liu, W., Grundler, P., and Brewe, D., 2008, Tracking the chemistry of ancient fluids: oxidation state of europium in hydrothermal scheelite: Chem Geol, v. 257, p. 26-33.

Brugger, J., Pring, A., Reith, F., Ryan, C., Etschmann, B., Liu, W., O'Neill, B., and Ngothai, Y., 2010, Probing ore deposits formation: New insights and challenges from synchrotron and neutron studies: Radiation Physics and Chemistry, v. 79, p. 151-161.

Bruker, A., 2005, TOPAS V3: General profile and structure analysis software for powder diffraction data: User's Manual, Bruker AXS, Karlsruhe, Germany.

Conradson, S. D., 1998, Application of X-ray absorption fine structure spectroscopy to materials and environmental science: Applied Spectroscopy, v. 52, p. 252A-252A.

Fritsche, R., and Dahlkamp, F., 1997, Contribution to characteristics of uranium oxides: Assessment of uranium deposit types and resources-a worldwide perspective. Proc Tech Comm Meeting, IAEA and OECD Nuclear Energy Agency, Vienna, 1997.

Goldstein, J., Newbury, D. E., Echlin, P., Joy, D. C., Romig Jr, A. D., Lyman, C. E., Fiori, C., and Lifshin, E., 2012, Scanning electron microscopy and X-ray microanalysis: a text for biologists, materials scientists, and geologists, Springer Science & Business Media.

Grønvold, F., 1955, High-temperature X-ray study of uranium oxides in the UO_2-U_3O_8 region: Journal of Inorganic and Nuclear Chemistry, v. 1, p. 357-370.

Kirkham, R., Dunn, P., Kuczewski, A., Siddons, D., Dodanwela, R., Moorhead, G., Ryan, C., De Geronimo, G., Beuttenmuller, R., and Pinelli, D., 2010, The Maia spectroscopy detector system: engineering for integrated pulse capture, low-latency scanning and real-time processing: American Institute of Physics Conference Series, 2010, p. 240-243.

Paterson, D., De Jonge, M., Howard, D., Lewis, W., McKinlay, J., Starritt, A., Kusel, M., Ryan, C., Kirkham, R., and Moorhead, G., 2011, The X‐ray Fluorescence Microscopy Beamline at the Australian Synchrotron: THE 10TH INTERNATIONAL CONFERENCE ON X‐RAY MICROSCOPY, 2011, p. 219-222.

Pecharsky, V. K., and Zavalij, P. Y., 2003, Fundamentals of Diffraction: Fundamentals of Powder Diffraction and Structural Characterization of Materials, p. 99-260.

Reimer, L., 2013, Transmission electron microscopy: physics of image formation and microanalysis, Springer.

Ryan, C., Kirkham, R., Hough, R., Moorhead, G., Siddons, D., De Jonge, M., Paterson, D., De Geronimo, G., Howard, D., and Cleverley, J., 2010, Elemental X-ray imaging using the Maia detector array: the benefits and challenges of large solid-angle: Nuclear Instruments and Methods in Physics Research Section A: Accelerators, Spectrometers, Detectors and Associated Equipment, v. 619, p. 37-43.

Ryan, C., Siddons, D., Kirkham, R., Li, Z., de Jonge, M., Paterson, D., Kuczewski, A., Howard, D., Dunn, P., and Falkenberg, G., 2014, MAIA X-ray fluorescence

imaging: capturing detail in complex natural samples: Journal of Physics: Conference Series, 2014, p. 012002.

Ryan, C., Siddons, D., Moorhead, G., Kirkham, R., De Geronimo, G., Etschmann, B., Dragone, A., Dunn, P., Kuczewski, A., and Davey, P., 2009, High-throughput X-ray fluorescence imaging using a massively parallel detector array, integrated scanning and real-time spectral deconvolution: Journal of Physics: Conference Series, 2009, p. 012013.

Ryan, C. G., Etschmann, B., Vogt, S., Maser, J., Harland, C., Van Achterbergh, E., and Legnini, D., 2005, Nuclear microprobe–synchrotron synergy: Towards integrated quantitative real-time elemental imaging using PIXE and SXRF: Nuclear Instruments and Methods in Physics Research Section B: Beam Interactions with Materials and Atoms, v. 231, p. 183-188.

Shavarov, Y. V., Bastrakov, E, 1999, HCh: a software package for geochemical equilibrium modelling (user's guide), p. 61.

Singh, Y., Viswanathan, R., Parihar, P. S., and Maithani, P. B., 2011, X-Ray crystallography of uraninite from proterozoic sedimentary basins of peninsular India: Implications for uranium ore genesis: The Indian Mineralogist, v. 45, p. 1-30.

Sweatman, T., and Long, J., 1969, Quantitative electron-probe microanalysis of rock-forming minerals: Journal of Petrology, v. 10, p. 332-379.

Wittry, D. B., 1958, Resolution of electron probe microanalyzers: Journal of Applied Physics, v. 29, p. 1543-1548.

Wülser, P.-A., Meisser, N., Brugger, J., Schenk, K., Ansermet, S., Bonin, M., and Bussy, F., 2005, Cleusonite,(Pb, Sr)(U^{4+}, U^{6+})(Fe^{2+}, Zn)$_2$ (Ti, Fe^{2+}, Fe^{3+})$_{18}$ (O, OH)$_{38}$, a new mineral species of the crichtonite group from the western Swiss Alps: European journal of mineralogy, v. 17, p. 933-942.

Yamamoto, Y., Takahashi, Y., Kanai, Y., Watanabe, Y., Uruga, T., Tanida, H., Terada, Y., and Shimizu, H., 2008, High-sensitive measurement of uranium L< sub> III</sub>-edge X-ray absorption near-edge structure (XANES) for the determination of the oxidation states of uranium in crustal materials: Applied Geochemistry, v. 23, p. 2452-2461.

Chapter 3

Uranium scavenging during mineral replacement reactions

Kan Li,[1] Allan Pring,[2,4] Barbara Etschmann,[1,2,7] Edeltraud Macmillan,[3] Yung Ngothai,[1] Brian O'Neill,[1] Anthony Hooker,[1,5] Fred Mosselmans,[6] and Joël Brugger[2,7*]

[1]School of Chemical Engineering and [3]School of Earth and Environmental Sciences, The University of Adelaide, 5000, South Australia, Australia

[2]Division of Mineralogy, South Australian Museum, North Terrace, 5000, Adelaide, South Australia, Australia

[4]School of Chemical and Physical Sciences, Flinders University, 5001, South Australia, Australia

[5]Radiation Health, Radiation Protection Branch, Environment Protection Authority, Victoria SQ, 5000, Adelaide, South Australia, Australia

[6]Diamond Light Source Ltd, Diamond House, Harwell Science and Innovation Campus, Didcot, Oxfordshire, UK, OX11, 0DE

[7]School of Earth, Atmosphere and Environment, Monash University, 3800, Clayton, Victoria, Australia

American Mineralogist, 2015, **100**, 1728-1735.

Statement of Authorship

Title of Paper	Uranium Scavenging during mineral replacement reactions.
Publication Status	Published
Publication Details	Li, K., Pring, A., Etschmann, B., Macmillan, E., Ngothai, Y., O'Neill, B., Hooker, A., Mosselmans, F. and Brugger, J. (2015) Uranium scavenging during mineral replacement reactions. American Mineralogist **100**, 1728-1735.

Principal Author

Name of Principal Author (Candidate)	Kan Li		
Contribution to the Paper	Designed and performed experiments, interpreted and processed data, wrote manuscript.		
Overall percentage (%)	85%		
Signature		Date	03 September 2015

Co-Author Contributions

By signing the Statement of Authorship, each author certifies that:

i. the candidate's stated contribution to the publication is accurate (as detailed above);
ii. permission is granted for the candidate in include the publication in the thesis; and
iii. the sum of all co-author contributions is equal to 100% less the candidate's stated contribution.

Name of Co-Author	Allan Pring		
Contribution to the Paper	Superivsed development of work, helped in data interpretation and manuscript evaluation.		
Signature		Date	04 September 2015

Name of Co-Author	Barbara Etschmann		
Contribution to the Paper	Superivsed development of work, helped in data interpretation and manuscript evaluation.		
Signature		Date	05 September 2015

!

Name of Co-Author	Edeltraud Macmillan		
Contribution to the Paper	Helped in data interpretation and manuscript evaluation.		
Signature		Date	03 September 2015

Name of Co-Author	Yung Ngothai		
Contribution to the Paper	Superivsed development of work, helped in data interpretation and manuscript evaluation.		
Signature		Date	04 September 2015

Name of Co-Author	Brian O'Neill		
Contribution to the Paper	Superivsed development of work, helped in data interpretation and manuscript evaluation.		
Signature		Date	04 September 2015

Name of Co-Author	Antony Hooker		
Contribution to the Paper	Superivsed development of work, helped in data interpretation and manuscript evaluation.		
Signature		Date	07 September 2015

Name of Co-Author	Fred Mosselmans		
Contribution to the Paper	Help in data interpretation and manuscript evalution.		
Signature		Date	04 Septermber 2015

Name of Co-Author	Joël Brugger		
Contribution to the Paper	Superivsed development of work, helped in data interpretation and manuscript evaluation, and acted as corresponding author.		
Signature		Date	05 September 2015

!

Li, K., Pring, A., Etschmann, B., Macmillan, E., Ngothai, Y., O'Neill, B., Hooker, A., Mosselmans, F. & Brugger, J. (2015). Uranium scavenging during mineral replacement reactions.
American Mineralogist, 100(8-9), 1728-1735.

Chapter 4

The exsolution of chalcopyrite from bornite digentite solid solution under hydrothermal conditions: an example of a back replacement reaction

Kan Li[1, 2], Joël Brugger[1,3], Yung Ngothai[2] and Allan Pring[1,4,*]

[1]Department of Mineralogy, South Australian Museum, North Terrace, Adelaide, SA 5000, Australia

[2]School of Chemical Engineering, University of Adelaide, Adelaide, SA 5005, Australia

[3]School of Earth, Atmosphere and the Environment, Monash University, Clayton, VIC 3800, Australia

[4]School of Chemical and Physical Science, Flinders University, Sturt Road, Bedford Park 5042, SA, Australia

Statement of Authorship

Title of Paper	The exsolution of chalcopyrite from bornite digentite solid solution under hydrothermal conditions: an example of a back replacement reaction
Publication Status	Publication Style
Publication Details	Li, K, Brugger, J, Ngothai. Y, and Pring A, The exsolution of chalcopyrite from bornite digentite solid solution under hydrothermal conditions: an example of a back replacement reaction, Preparing for submission to be a geochemistry journal.

Principal Author

Name of Principal Author (Candidate)	Kan Li		
Contribution to the Paper	Designed and performed experiments, interpreted and processed data, wrote manuscript.		
Overall percentage (%)	70%		
Signature		Date	10 November 2015

Co-Author Contributions

By signing the Statement of Authorship, each author certifies that:

i. the candidate's stated contribution to the publication is accurate (as detailed above);
ii. permission is granted for the candidate in include the publication in the thesis; and
iii. the sum of all co-author contributions is equal to 100% less the candidate's stated contribution.

Name of Co-Author	Joël Brugger		
Contribution to the Paper	Superivsed development of work, helped in data interpretation and manuscript evaluation.		
Signature		Date	10 November 2015

Name of Co-Author	Yung Ngothai		
Contribution to the Paper	Superivsed development of work, helped in data interpretation and manuscript evaluation.		
Signature		Date	12 November 2015

!

Name of Co-Author	Allan Pring		
Contribution to the Paper	Superivsed development of work, helped in data interpretation and manuscript evaluation.		
Signature		Date	11 November 2015

Please cut and paste additional co-author panels here as required.

4.1 Abstract

We report on the formation of chalcopyrite exsolution lamellae from the breakdown of a bornite-digenite solid solution (*bdss*) originally formed via replacement of a parent chalcopyrite grain under hydrothermal conditions. The exsolution is a back reaction which occurred during low temperature annealing at 150 °C following the initial replacement of chalcopyrite by *bdss* at 300 ˚C in a solutions nominally containing Cu(I) and hydrosulfide in a $pH_{25°C}$ ~6 acetate buffer. The progress of the back-reaction is catalyzed by small amounts of fluid present in the porosity within *bdss*; this porosity results from the formation of *bdss* via the replacement of chalcopyrite by bornite-digenite following an interface coupled dissolution reprecipitation mechanism. The chalcopyrite lamellae show a strong crystallographic dependence for orientation and are surrounded by regions of digenite. Simultaneously to its breakdown to chalcopyrite and digenite, *bdss* is also breaking down to fine grained bornite plus digenite via exsolution. These experimental results are consistent with naturally observed textures where lamellae of chalcopyrite are observed around cracks and fractures in bornite that has been formed via replacement of chalcopyrite. This confirms experimentally that bornite can replace chalcopyrite, and chalcopyrite can replace bornite under hydrothermal conditions over very short times (days). The experiments also show that these reactions are controlled by kinetic factors (e.g., relative nucleation rates of Cu-Fe-sulfides; presence of porosity) rather than equilibrium thermodynamics.

Keywords: chalcopyrite, bornite, mineral replacement, hydrothermal, bornite-digenite solid solution.

4.2 Introduction

Chalcopyrite ($CuFeS_2$) and bornite (Cu_5FeS_4) are the most abundant primary Cu-bearing sulfides across a wide range of ore deposit types. Both minerals are part of the same broad sulfide structural family with their structures being derived from zinc blende; a cubic close-packed array of S atoms with metal cations (Cu and Fe) occupying some of the available tetrahedral sites in the S lattice.

Recently Zhao et al. (2014a) undertook a detailed experimental study of the replacement of chalcopyrite by bornite under hydrothermal conditions, and found that the composition of the bornite product (in reality compositions in the bornite-digenite solid solution (*bdss*)) depended principally on the temperature of the reaction rather than solution composition, with end-member bornite forming at 320 °C while compositions close to $Bn_{60}Dg_{40}$ formed at 240 °C. In other experiments in which chalcopyrite and bornite were formed by the replacement of hematite in Cu(I)- and hydrosulfide-bearing fluids, bornite only formed as a secondary replacement of chalcopyrite rather than direct replacement of hematite, even under conditions where chalcopyrite is the thermodynamically stable phase (Zhao et al., 2014b).

In nature, the majority of chalcopyrite and bornite intergrowths have textures consistent with fluid-mediated replacement reactions (Ramdohr, 1980; Robb, 2013), but some chalcopyrite-bornite assemblages have been interpreted in terms of solid-state exsolution or unmixing processes, e.g. bornite intergrown with a maze of minute chalcopyrite needles (Cook et al., 2011; Ramdohr, 1980). Here, we investigate the formation of chalcopyrite lamellae during the replacement of chalcopyrite by bornite under hydrothermal conditions at

300 °C and 90 bar, and *in situ* annealing in the unquenched hydrothermal fluid at 150 °C. The aim is to establish the formation mechanism of the chalcopyrite lamellae.

4.3 Samples and methods

Chalcopyrite from Wallaroo Mines, South Australian (SA Museum sample G22621) was used as starting material throughout this study. This chalcopyrite sample was also used by Zhao et al. (2014a) and shown to be phase pure and have an average composition $Cu_{1.04(8)}Fe_{1.05(2)}S_{1.91(4)}$. Following the method of Zhao et al. (2014a) the chalcopyrite was crushed, washed, and sieved into a 125 to 150 µm size fraction. Analytical grade reagents were used throughout. A $pH_{25°C}$ ~6 acetate buffer solution was prepared by adding 0.055 m CH_3COOH and 0.955 m CH_3COONa. The presence of the H_2S, generated from the breakdown of thioacetamide above 100 °C, gave an effective pH at 300 °C of 5.88 calculated using the HCh geochemical modeling software (Shavarov, 1999). For each run, 10 mg of chalcopyrite crystal fragments (55 µmoles), 21.5 mg CuCl(s) (217 µmoles), 0.1890 g thioacetamide (liberating ~0.5 molal S into solution) and 5 mL reaction solution were carefully measured and added into an 8 mL titanium autoclave in an argon-filed anoxic glove box. One molar equivalent of NaCl was added to the solution to stabilize Cu(I) (Brugger et al., 2007). In some runs 300 ppm U^{6+} in the form of $UO_2(NO_3)_2$(s) was added to the solution, but otherwise the experimental conditions were identical to the U-free runs. The sealed cells were left in electric Muffle furnaces (temperature regulation ±2 °C) for 4 days at 300 °C and then the temperature lowered to 150 °C. The cooling in the furnace from 300 to 150 °C took less than 10 minutes. During the experiments, the pressures in the autoclaves were autogenous, i.e. around 90 bar at 300 °C. After annealing at 150 °C for 2 days the cells were quenched to room temperature in a large volume of cold water (~10 L) for 20 minutes. The solids were rinsed three times using Milli-Q water, then once using

acetone, and left to dry in a desiccator over silica gel at room temperature for several days. Some samples were embedded in epoxy resin and polished for textural examination; others were crushed for powder XRD analysis.

The nature and proportions of the phases were determined by Rietveld quantitative phase analysis (QPA) of powder X-ray diffraction data with the program Topas (Bruker, 2005), using diffraction data in the 2θ range from 4 to 100° (Co Kα_1 X-radiation), following the procedure described by Zhao et al. (2014b). The characterization of the textures of the products was undertaken using a FEI Quanta 450 field emission scanning electron microscope (FESEM) at Adelaide Microscopy, University of Adelaide. The chemical compositions of the products were determined using the EDS detector system on the FESEM and calibrated against the Wallaroo Mines chalcopyrite. A natural sample of chalcopyrite partially replaced by bornite from the Moonta Mines, South Australia (S.A. Museum G 23265) was used for textural comparison.

4.4 Results and Discussion

Under the solution conditions explored in this study, chalcopyrite was replaced by a bornite-rich composition in the *bdss* with bulk composition corresponding to $Bn_{85}Dg_{15}$, in keeping with the findings of Zhao et al. (2014a). *Bdss* formed both via replacement of chalcopyrite following and interface couple dissolution-reprecipitation mechanism, and via overgrowth. After a period of 4 days reaction at 300 °C, the temperature in the furnace was dropped to 150 °C, and the sample was annealed for 2 days at this temperature. After this time, the sample was quenched to room temperature.

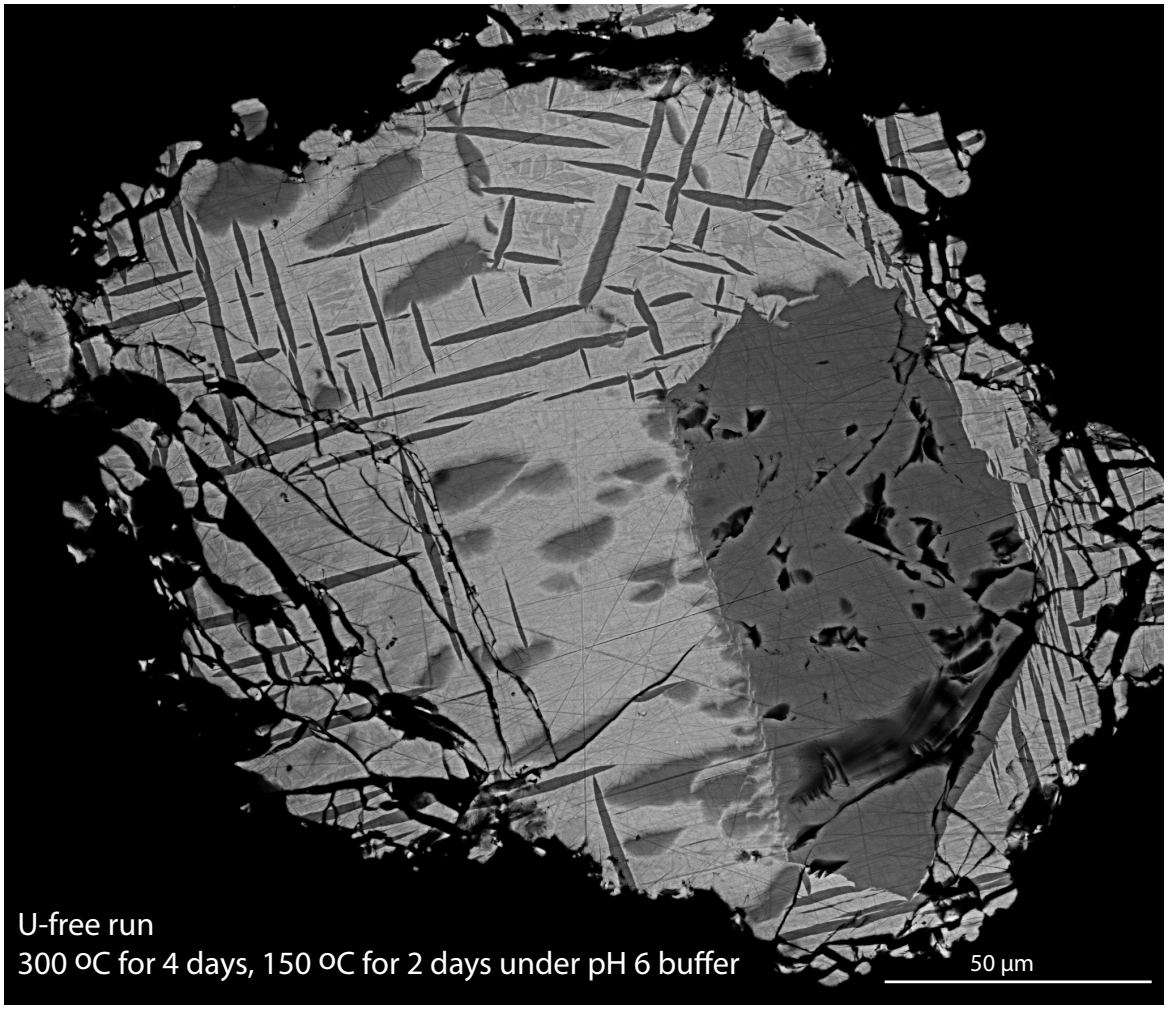

Figure 1 SEM image of reaction product from chalcopyrite. The reaction was conducted in a pH25˚C 6 acetate buffer and I m NaCl at 300 ^{o}C for 4 days, and at 150 ^{o}C for 2 days.

Figure 1 shows a section of a grain in which the initial transformation of chalcopyrite to *bdss* did not go to completion during the synthesis step. A large remnant of parent chalcopyrite remains within the *bdss* matrix (bottom right of the grain), but is completely surrounded by a rim of *bdss*. In addition to the unreacted core of chalcopyrite, there are a number of sharp lamellae (to 50 µm in length) and some triangular to rectangular patches (to 40 µm) across other parts of the grain. EDS analyses show that the patches have a composition $Cu_{1.09(3)}Fe_{0.94(3)}S_2$, consistent with chalcopyrite. The sharp lamellae give a Cu-rich chalcopyrite composition $Cu_{1.3(1)}Fe_{0.8(1)}S_2$; the high Cu value and large uncertainties in the lamellae analysis likely reflect the effects of beam spread into the neighboring *bdss*

matrix. The powder XRD data shows that the chalcopyrite from U-free experiments gives a broader set of reflections, which indicates chalcopyrite phases include multi compositions after reactions. Table 1 provides a summary of the QPA data for the synthetic sample.

Table 1 Summary of the QPA data for the synthetic samples

	Chalcopyrite			**Bornite**		**Digenite**	
	Starting	U-free	300ppm U	U-free	300ppm U	U-free	300ppm U
wt% (±3)	-	16.41	10.18	42.25	59.49	41.34	30.33
Peak Width (2θ)	0.094(1) (34.32)	0.129(2) (34.31)	0.0834(7) (34.32)	0.193(5) (55.10)	0.160(17) (55.11)	0.264(2) (54.58)	0.296(3) (54.41)
Refined-cell parameters (Å)	a: 5.2890(3) c: 10.423(4)	a:5.2898(5) c:10.4177(14)	a: 5.2916(4) c: 10.4223(11)	a:10.9519(7)	a:10.9576(5)	a:5.5264(3)	a: 5.5417(6)
Notes: structure models from ICSD data base Chalcopyrite #94554, Bornite #24174, Digenite #42709							

Figure 2 is a BSE image of a fully replaced chalcopyrite grain with a geometric network of sharp chalcopyrite lamellae, the longest of which are approximately 50 µm. The regular geometric relationship of the lamellae is constrained by the crystallographic orientation of the original grain boundaries of both the primary chalcopyrite grain (which has been transformed to *bdss*) and *bdss* overgrowth (Zhao et al., 2014b). In addition there are two parallel broader strips or patches of chalcopyrite, which are both wider and have more diffuse edges than the lamellae. Initially, these were thought to be remnants of unreacted chalcopyrite, but their geometry in both Figures 1 and 2 is consistent with an oblique angle intersection of the sharp lamellae, which will be disk-shaped in 3 dimensions. These less regular lamellae also occur in the overgrowth bornite matrix, which would be free of primary chalcopyrite. There is a significant difference in the size and density of the chalcopyrite lamellae in the core of the grain (*bdss* formed via replacement of chalcopyrite) and in the rim (*bdss* formed by overgrowth), with the lamellae in the rim between shorter and higher density. This is despite the fact that the *bdss* composition of the core and overgrowth are indistinguishable (Zhao et al., 2014b).

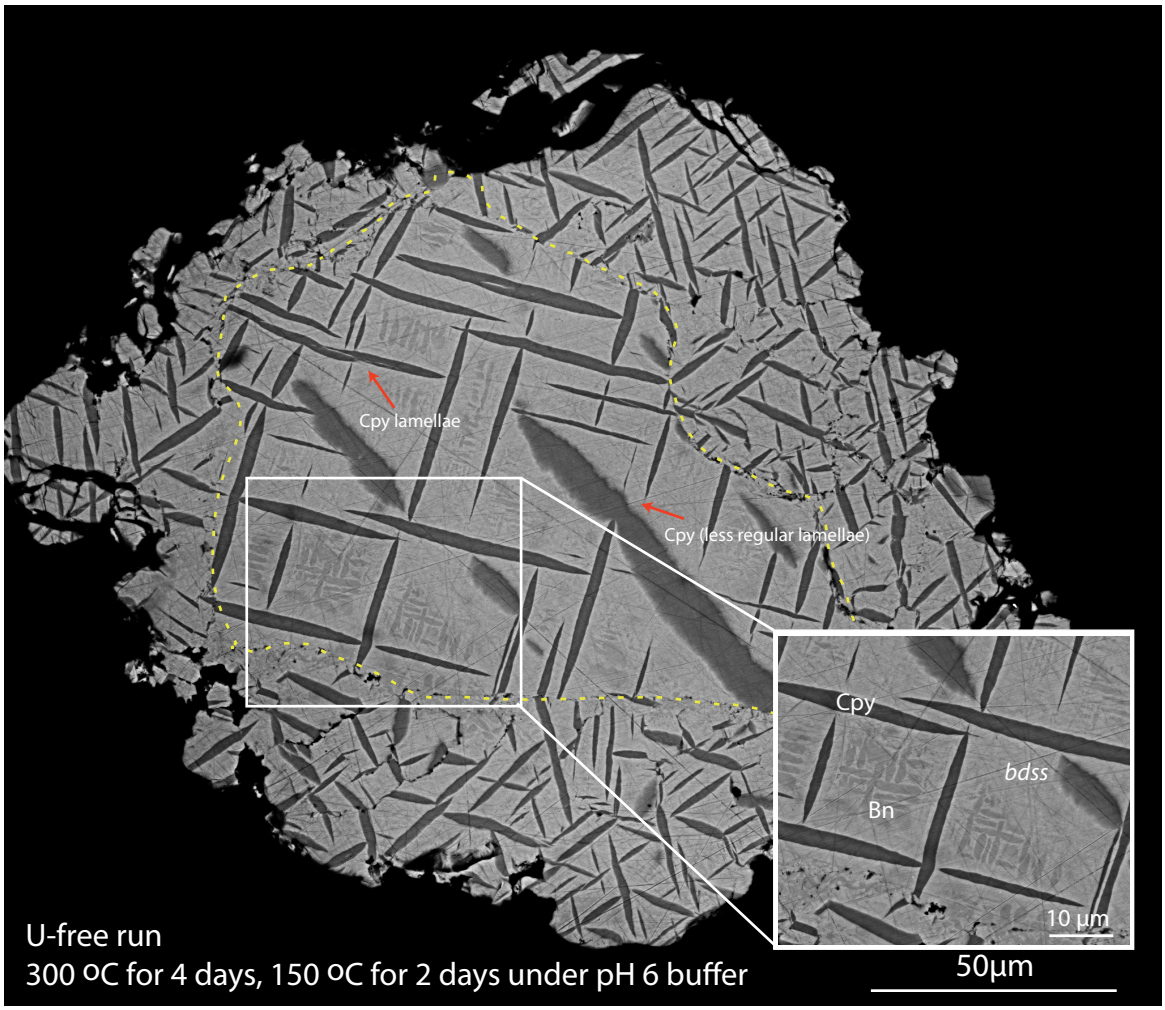

Figure 2 SEM image of reaction product from chalcopyrite (fully replaced). The reaction was conducted in a $pH_{25°C}$ 6 acetate buffer and I m NaCl at 300 °C for 4 days, and at 150 °C for 2 days.

In both Figures 1 & 2, in the regions between the chalcopyrite lamellae there is a finer network of small lamellae (~2 to 5 µm in length) of a lighter shade of grey, which, based on EDS analyses and the powder XRD data in Table 1, are bornite lamellae. The chalcopyrite lamellae are separated from the finer bornite lamellae by what appears to be an area of Cu-enrichment, as indicated by the contrast in the BSE imaging. This feature is much clearer in Figure 3, which shows a *bdss* grain formed by replacement of chalcopyrite with 300 ppm U^{6+} in solution. The U precipitates out as UO_{2+x} as a rim around the boundary of the parent grain (see Li et al., 2015). The UO_{2+x} rim separates areas of *bdss* overgrowth from the parent grain. Many of the features noted in Figures 1 &2 are exemplified in Figure 3. The

chalcopyrite lamellae are larger, up to 100 µm in length in the core of the grain, and Cu-enriched regions surrounding the chalcopyrite lamellae are clear. EDS analyses for the chalcopyrite lamellae give a composition $Cu_{1.14(1)}Fe_{0.97(1)}S_2$ and for the Cu-enriched regions $Cu_{7.1(7)}Fe_{0.5(1)}S_5$, the latter being close to digenite. Finer bornite lamellae give an almost stoichiometric bornite composition $Cu_{5.05(2)}Fe_{0.92(2)}S_4$.

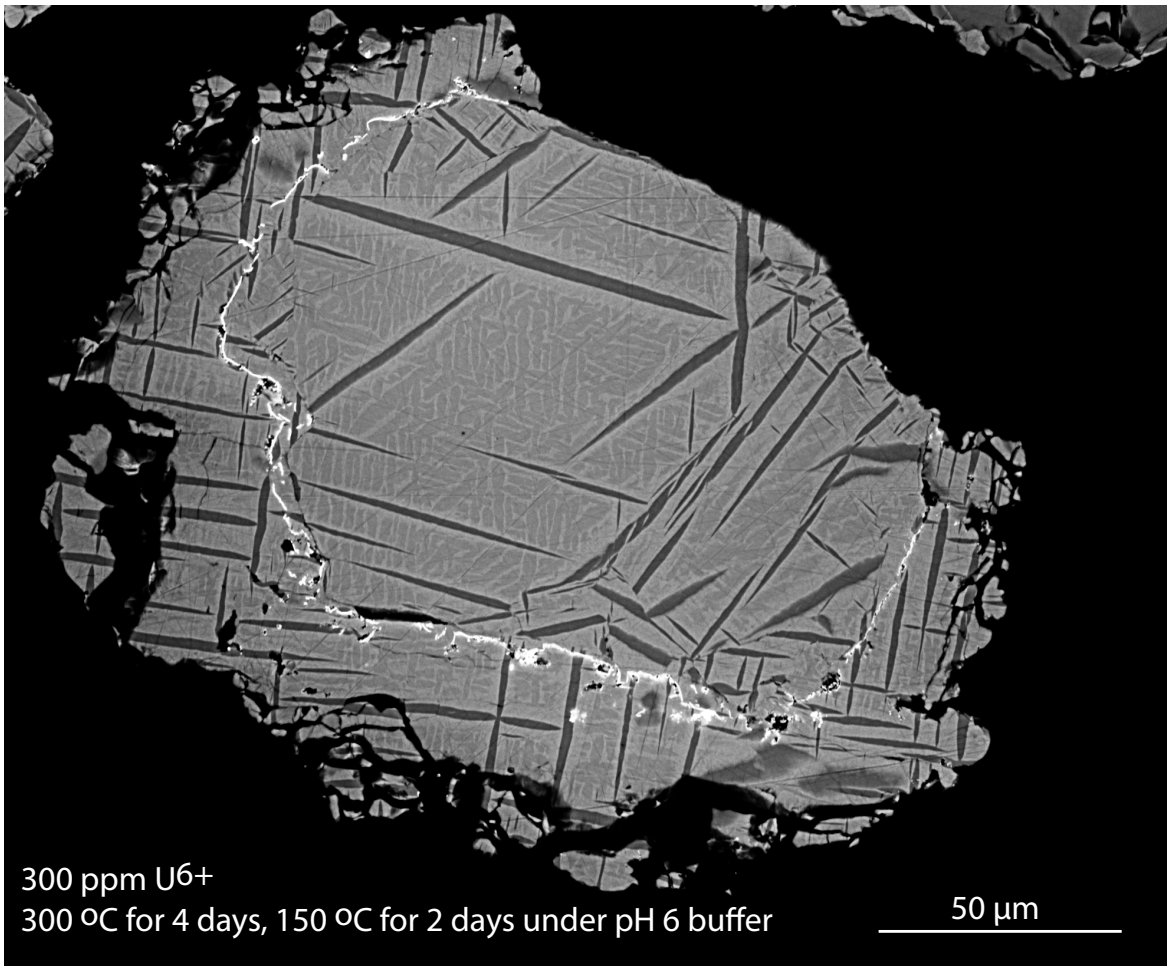

Figure 3 SEM image of reaction product from chalcopyrite with 300ppm U^{6+}. The reaction was conducted in a $pH_{25°C}$ 6 acetate buffer and I m NaCl at 300 °C for 4 days, and at 150 °C for 2 days.

The chalcopyrite lamellae textures noted above are very similar to those observed in some natural samples, where chalcopyrite has been replaced by bornite, and back reaction has caused chalcopyrite lamellae to form. An example of such a texture from the Moonta Mines, South Australia, is illustrated in Figure 4, which shows a vein of bornite formed within

massive chalcopyrite. Open cracks and fractures are present within the bornite vein, and lamellae of chalcopyrite have formed along these active fluid flow sites.

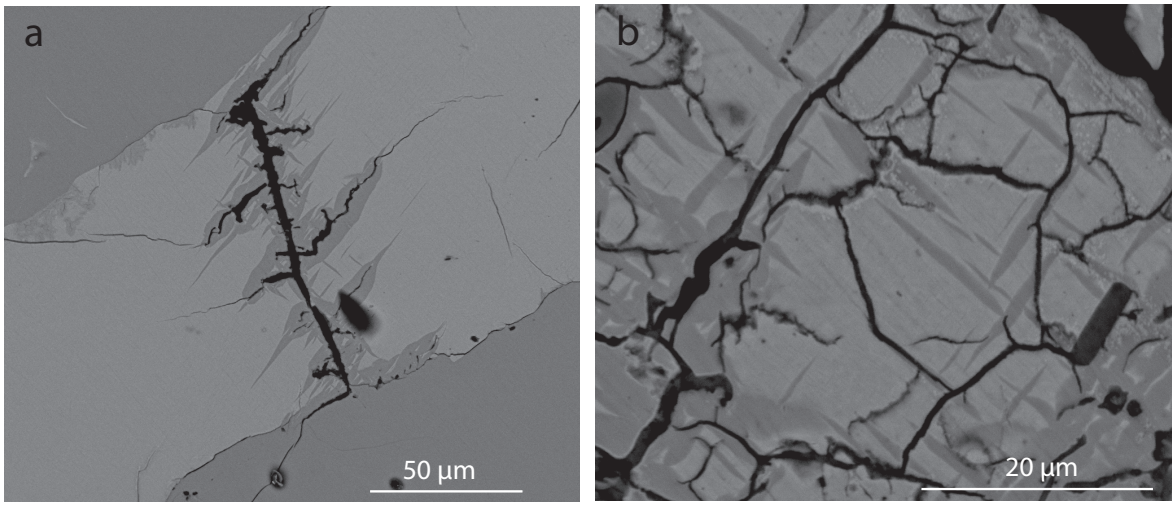

Figure 4 (a) a vein of bornite (light grey) through massive chalcopyrite (darker grey) In the centre of the bornite vein are a network of cracks which are lined with chalcopyrite indicating back replacement of bornite by chalcopyrite where there was active fluid flow. Sample from Moonta Mines, SA. (b) Enlargement of a slightly different area of the same sample in which chalcopyrite replacement of bornite is clear along cracks and also is a network of orthogonal "spear tip shaped" lamella of secondary chalcopyrite. Note also the mottled texture in the bornite wich indicates it might be breaking down to digenite

In the synthetic grains the exsolution processes appear to preserve both the bulk composition and the overall volume of the grains. The uncertainties in the EDS analyses are increased by the relatively fine-grained nature of the textures (from an electron beam analysis point of view) and precludes writing accurate chemical equations for the process, but in general terms there are two competing exsolution processes:

$$bdss \rightarrow \text{cpy} + \text{dg} \quad (1)$$

and

$$bdss \rightarrow \text{bn} + \text{dg}. \quad (2)$$

Zhao et al. (in prep) observed only the second of these reactions in their detailed study of the role of fluids and porosity in accelerating the kinetics of exsolution reactions in the *bdss*. These experiments were conducted under similar conditions to those described in this paper,

expect for the use of basic borate buffer (nominal $pH_{25°C}$ of 10) rather than the slightly acidic acetate buffer ($pH_{25°C}$ ~6) used in our study. This dependence of the nature of the exsolution reaction on bulk solution pH indicates that the solution plays a fundamental role in driving the unmixing process. Equation (3) shows that a simplified unmixing reaction (stoichiometric compositions of digenite and chalcopyrite) does not depend on pH, and is associated with a volume decrease of ~16%. In reality, the replacement appears to be near isovolumetric, which can be represented by equation (4); in this case, a lower pH would favor the unmixing. Equation (5) shows the dissolution of *bdss*, which is favored by high pH. However, equation (5) is unlikely to provide a useful guide in predicting reaction pathways in this system, since it involves the reduction of S in digenite; this is unlikely to happen via the release of molecular oxygen, but rather via S chemistry. Hence, in detail, the effect of pH and other solution parameters on reaction outcome may be controlled by local disequilibrium chemistry at mineral interface, which is affected only indirectly by the bulk fluid composition. Equation (6) presents the dissolving of Cu in the solution to drive the formation of chalcopyrite to keep the balance of Fe in solid. In this system, total volume decreases around 19%.

[Fe and Cu immobile; 45 vol% cpy product; volume decrease of 14%]

$$Bn_{0.85}Dg_{0.15} + 0.19\ H_2S(aq) + 0.09\ O_2(g) = 0.53\ Dg + 0.85\ Cpy + 0.19\ H_2O \quad (3)$$

[Fe immobile; isovolume -> 38 vol% cpy product]

$$Bn_{0.85}Dg_{0.15} + 1.67\ Cu(HS)_2^- + 1.67\ H^+ + 0.14\ O_2(g) = 0.71\ Dg + 0.85\ Cpy + 2.22\ H_2S(aq) + 0.28\ H_2O \quad (4)$$

[Dissolution of bdss]

$$Bn_{0.85}Dg_{0.15} + 1.35\ H_2O + 7.05\ H_2S(aq) = 5.60\ Cu(HS)_2^- + 0.85\ FeCl_2(aq) + 5.60\ H^+ + 0.68\ O_2(aq) \quad (5)$$

[Fe and S preserved; 47% cpy product; volume decrease of 19%]

$$Bn_{0.85}Dg_{0.15} + 0.68\ H_2S(aq) + 0.08\ O_2(g) = 0.49\ Dg + 0.85\ Cpy + 0.34\ Cu(HS)_2^- + 0.34\ H^+ + 0.17\ H_2O \quad (6)$$

Zhao et al. (2014a) demonstrated that the replacement of chalcopyrite by *bdss* in an ICDR reaction, and that porosity plays an important role in driving the reaction (see also Altree-Williams et al., 2015). Milke et al. (2013) and Zhao et al. (in prep) also found that fluids located in fluid inclusions or grain boundaries play a first order role in accelerating the kinetics of mineral reactions by several orders of magnitude compared to dry systems.

There are also some pores, particularly around the rim marking the outline of the original chalcopyrite grains illustrated in the figures, but much of the porosity generally observed in ICDR reactions, and vital for fluid and mass transport during the reactions, seems to have been healed during the exsolution process. This suggests that the exsolution process closes the pores and points to thin layers of solution at the exsolution interface. Alternatively, the water may be present along grain boundaries, not forming a separate phase, as inferred in Milke et al. (2013) experiments. In both cases, water drives the unmixing reaction by accelerating mass transport between the lamellae and the matrix at the interface. In our experiments where the system temperature is lowered to annealing temperature, one expects the permeability of the system to remain open to the bulk solution during the exsolution. This could facilitate changes in the bulk composition of the solid during the unmixing reaction, but our EDS and XRD measurements suggest that this does not happen to any significant extent. The fluid content of the solid at the end of the reaction is difficult to measure accurately in these sulfide systems, but estimates by Zhao et al. (in prep), based on measuring the area of fluid inclusion on fractured surfaces by SEM, give an estimated maximum fluid content of 3,000 ppm.

In the natural sample from Moonta showing chalcopyrite lamellae in the bornite matrix (Figure 4), it is notable that these are closely associated with a network of microcracks and fractures. Here it is clear that the overall volume of the system is contracting indicating that the bornite to chalcopyrite reaction is driven by the loss of Cu to solution like equation (6), rather than the addition of Fe to the system.

4.5 Final words

This work confirms that fluid can play an important role in 'exsolution' reactions, particularly when the overall mineral formation reaction is an interface coupled dissolution reprecipitation reaction. Hence, for natural materials, 'exsolution' should be use to describe a particular texture, rather than imply a solid-state diffusion-driven reaction mechanism, which in most cases cannot be demonstrated. The fact that the nature of the exsolution products is pH-dependent indicates that fluid composition plays an important role in controlling not only the kinetics of the reaction, but also the nature of the exsolution products. The breakdown of the *bdss* in this case involved two separate, probably simultaneous and competing reactions (*bdss* to cpy and *bdss* to bn and dg) is a strong indication that this system is not in equilibrium. The chalcopyrite exsolution in natural bornite from Moonta indicate that this type of reaction occurs in nature. In keeping with the conclusions of Milke et al. (2013)and Zhao et al. (in prep), we suggest that the catalysis of 'exsolution' reaction by the presence of small amounts of fluids is common in minerals, and that this may be the prominent mechanism facilitating 'exsolution' reaction in hydrothermally formed ore minerals.

4.6 Acknowledgement

We thank, Aoife McFadden, and Benjamin Wade from Adelaide Microscopy Center for their assistance in using the FESEM and electron microprobe. This work has been made possible by the financial support of the Australian Research Council (Grants DP0880884 and DP1095069).

7 References

Altree-Williams, A., Pring, A., Ngothai, Y., and Brugger, J., 2015, Textural and compositional complexities resulting from coupled dissolution-reprecipitation reactions in geomaterials: Earth-Science Review, in press.

Brugger, J., Etschmann, B., Liu, W., Testemale, D., Hazemann, J.-L., Emerich, H., Van Beek, W., and Proux, O., 2007, An XAS study of the structure and thermodynamics of Cu (I) chloride complexes in brines up to high temperature (400 C, 600bar): Geochimica et Cosmochimica Acta, v. 71, p. 4920-4941.

Bruker, A., 2005, TOPAS V3: General profile and structure analysis software for powder diffraction data: User's Manual, Bruker AXS, Karlsruhe, Germany.

Cook, N. J., Ciobanu, C. L., Danyushevsky, L. V., and Gilbert, S., 2011, Minor and trace elements in bornite and associated Cu–(Fe)-sulfides: A LA-ICP-MS studyBornite mineral chemistry: Geochimica et Cosmochimica Acta, v. 75, p. 6473-6496.

Li, K., Pring, A., Etschmann, B., Macmillan, E., Ngothai, Y., O'Neill, B., Hooker, A., Mosselmans, F., and Brugger, J., 2015, Uranium scavenging during mineral replacement reactions: American Mineralogist, v. 100, p. 1728-1735.

Milke, R., Neusser, G., Kolzer, K., and Wunder, B., 2013, Very little water is necessary to make a dry solid silicate system wet: Geology, v. 41, p. 247-250.

Ramdohr, P., 1980, The Ore Minerals and Their Intergrowths, 2nd edn. International Series in Earth Science, 35, London: Pergamon Press.

Robb, L., 2013, Introduction to ore-forming processes, John Wiley & Sons.

Shavarov, Y. V., Bastrakov, E, 1999, HCh: a software package for geochemical equilibrium modelling (user's guide), p. 61.

Zhao, J., Brugger, J., Chen, G., Ngothai, Y., and Pring, A., 2014b, Experimental study of the formation of chalcopyrite and bornite via the sulfidation of hematite: Mineral replacements with a large volume increase: American Mineralogist, v. 99, p. 343-354.

Zhao, J., Brugger, J., Grguric, B. A., Ngothai, Y., and Pring, A., 2015, The fluid catalyzed unmixing behavior and alternative to exsolution processes in hydrothermal systems: the bornite-digenite solid solution (In prep).

Zhao, J., Brugger, J., Ngothai, Y., and Pring, A., 2014a, The replacement of chalcopyrite by bornite under hydrothermal conditions: American Mineralogist, v. 99, p. 2389-2397.

Chapter 5

Ore petrography using megapixel X-ray imaging: Rapid insights into element distribution and mobilisation in complex Pt and U-Ge-Cu ores

Kan Li[1], Barbara Etschmann[2], Nicholas Rae[2,3], Frank Reith[4,5], Chris G. Ryan[6], Robin Kirkham[7], Daryl Howard[3], Diogo R.N. Rosa[8], Carla Zammit[9], Allan Pring[10], Yung Ngothai[1], Antony Hooker[1,11], and Joël Brugger[2*1]

[1]School of Chemical Engineering and [5]School of Biological Sciences, The University of Adelaide, 5000, Adelaide, Australia

[2]School of Earth, Atmosphere and Environment, Monash University, 3800, Clayton, Australia

[3]Australian Synchrotron, Blackburn Road, Clayton, 3180, Australia

[4]The University of Adelaide, School of Biological Sciences, Waite Campus, Urrbrae, 5064, Australia

[5]CSIRO Land and Water, PMB2, Glen Osmond, South Australia 5064, Australia; [6]CSIRO Minerals Resources Flagship, Bayview Ave, Clayton, 3168, Australia; and [7]CSIRO Manufacturing Flagship, Bayview Ave, Clayton, 3168, Australia

[8]Department of Petrology and Economic Geology, Geological Survey of Denmark and Greenland, Øster Voldgade 10, Copenhagen K 1350, Denmark

[9]University of Queensland, School of Earth Sciences, St. Lucia, Brisbane, 4072, Australia

[10]School of Chemical and Physical Sciences, Flinders University, 5001, Adelaide, Australia

[11]Radiation Health, Radiation Protection Branch, Environment Protection Authority, Victoria SQ, 5000, Adelaide, Australia

Statement of Authorship

Title of Paper	Ore petrography using megapixel X-ray imaging: Rapid insights into element distribution and mobilisation in comples Pt and U-Ge-Cu ores
Publication Status	Accepted for publication
Publication Details	Li, K., Etschmann, B., Rae, N., Reith, F., Ryan, C.G., Kirkham, R., Howard, D., Rosa, D., Zammit, C., Pring, A., Ngothai, Y., Hooker, A. and Brugger, J. Ore petrography using megapixel X-ray imaging: Rapid insights into element distribution and mobilisation in complex Pt and U-Ge-Cu ores. Economic Geology.

Principal Author

Name of Principal Author (Candidate)	Kan Li		
Contribution to the Paper	Designed and performed experiments, interpreted and processed data, wrote manuscript.		
Overall percentage (%)	70%		
Signature		Date	03 September 2015

Co-Author Contributions

By signing the Statement of Authorship, each author certifies that:

i. the candidate's stated contribution to the publication is accurate (as detailed above);
ii. permission is granted for the candidate in include the publication in the thesis; and
iii. the sum of all co-author contributions is equal to 100% less the candidate's stated contribution.

Name of Co-Author	Barbara Etschmann		
Contribution to the Paper	Superivsed development of work, helped in data interpretation and manuscript evaluation.		
Signature		Date	04 September 2015

Name of Co-Author	Nicholas Rae		
Contribution to the Paper	Helped in data interpretation and manuscript evaluation.		
Signature		Date	04 September 2015

!

Name of Co-Author	Frank Reith		
Contribution to the Paper	Superivsed development of work, helped in data interpretation and manuscript evaluation.		
Signature		Date	03 September 2015

Name of Co-Author	Chris G.Ryan		
Contribution to the Paper	Superivsed development of work, helped in data interpretation and manuscript evaluation.		
Signature		Date	04 September 2015

Name of Co-Author	Robin Kirkham		
Contribution to the Paper	Helped in data interpretation and manuscript evaluation.		
Signature		Date	05 September 2015

Name of Co-Author	Daryl Howard		
Contribution to the Paper	Help in data interpretation and manuscript evalution.		
Signature		Date	03 September 2015

Name of Co-Author	Diogo R.N. Rosa		
Contribution to the Paper	Provided samples for experiments, helped in data interpretation and manuscript evaluation.		
Signature		Date	06 September 2015

Name of Co-Author	Carla Zammit		
Contribution to the Paper	Provided samples for experiments, and manuscript evaluation.		
Signature		Date	10 September 2015

Name of Co-Author	Allan Pring		
Contribution to the Paper	Superivsed development of work, helped in data interpretation and manuscript evaluation.		
Signature		Date	04 September 2015

Name of Co-Author	Yung Ngothai		
Contribution to the Paper	Superivsed development of work, helped in data interpretation and manuscript evaluation.		
Signature		Date	04 September 2015

Name of Co-Author	Antony Hooker		
Contribution to the Paper	Superivsed development of work, helped in data interpretation and manuscript evaluation.		
Signature		Date	04 September 2015

Name of Co-Author	Joël Brugger		
Contribution to the Paper	Superivsed development of work, helped in data interpretation and manuscript evaluation, and acted as cooresponding author.		
Signature		Date	04 September 2015

Li, K., Etschmann, B., Rae, N., Reith, F., Ryan, C.G., Kirkham, R., Howard, D., Rosa, D.R.N., Zammit, C., Pring, A., Ngothai, Y., Hooker, A. &Brugger, J.
Ore petrography using megapixel X-ray imaging: Rapid insights into element distribution and mobilisation in complex Pt and U-Ge-Cu ores.
Economic Geology, *111*(2), 487-501.

Chapter 6

Conclusion

The major contribution of this Ph.D thesis is to demonstrate the scavenging of uranium from hydrothermal fluids during ICDR reactions thus helping to elucidate the Cu-U association in IOCG deposits. Two sets of experimental studies on U-scavenging in Fe-Cu-S system are presented in detail: the replacement of hematite by chalcopyrite, and the transition between chalcopyrite and bornite. The second contribution is that this thesis provides an insight into the application of Megapixel-synchrotron X-ray fluorescence (MSXRF) for mapping the distribution of U from different types of U deposit. This chapter draws brief conclusions for each system studied, reviews the contribution of each project, and highlights the possible future research opportunities.

6.1 Mechanisms of uranium scavenging in mineral replacement reactions

In mineral replacement reactions in the Fe-Cu-S system, the uranium scavenging was mainly associated with the presence of HS^- in solution, resulting in a thin U-rich front marking the original hematite grain surface. This 'front' consists of nanocrystals of $UO_{2+x}(s)$, based on chemical mapping and XANES spectroscopy. This study also indicates the presence of different U-sources can affect the pathway of ICDR reactions.

6.1.1 Uranyl nitrate as uranium source

When uranyl nitrate is the uranium source of replacement reactions in Fe-Cu-S system, a key feature of these experiments is the presence of U-rich layers formed by an accumulation of $UO_{2+X}(S)$. The pathway of reactions starting from hematite also could be affected by the presence of U^{6+} in solution in contrast with U-free runs. Experimental results confirm the role of uranyl ions in the formation of pyrite. Pyrite did not form in the U-free run, due to absence of uranyl ions which are surmised to be the oxidant necessary for the formation of

pyrite. This outcome provides an adequate mechanism to explain the coupling between pyrite formation and uraninite precipitation. When uranyl nitrate was added into the reaction with chalcopyrite as a starting material, the U precipitates out as UO_{2+x} as a rim separating areas of *bdss* overgrowth from the parent grain, but there are otherwise no other differences in textures and phases from U-free runs. U-scavenging here is mainly caused by the presence of concentrated HS^- at the reaction front.

6.1.2 UO_{2+x} as uranium source

The replacement reaction from hematite to chalcopyrite where U was added as solid UO_{2+X}(s), differed from the U-free experiments. The hematite cores displayed porosity and patchy areas of pyrite and magnetite, since insoluble Fe^{3+} can be reduced to soluble Fe^{2+} in the presence of U^{4+} from solid UO_{2+X}(s), which can be oxidized to uranyl complexes at the same time. Then U^{6+} (aq) could join in the succeeding reactions as with uranyl nitrate. However, there is no evidence to indicate that the solid UO_{2+X} could join the reactions of exsolution of chalcopyrite from *bdss*. Thus, it can be concluded that the U-scavenging from the solid UO_{2+X} in Fe-Cu-S system only could occurs in the presence of oxidant.

6.2 Dissolution-reprecipitation and exsolution reactions

The investigation of U scavenging in Fe-Cu-S system also involves other two processes, dissolution-reprecipitation and exsolution.

In Chapter 3 it was demonstrated that chalcopyrite could be synthesized by the sulfidation of hematite with Cu(I) solution under hydrothermal conditions, and this is similar to the phenomenon observed by Zhao et al. (2014). However, the presence of a U-source helps hematite to be replaced by pyrite first, and chalcopyrite could subsequently form by the

replacement of pyrite. This outcome indicates the pathways of ICDR reactions are affected by amounts of minor elements.

The CDR reaction from chalcopyrite to bornite was presented in Chapter 4. Under hydrothermal conditions, chalcopyrite could be replaced by bornite at temperatures up to 300 ^{o}C. The sharp reaction front between chalcopyrite and bornite in grains is strong evidence of this reaction following a CDR mechanism. Furthermore, this study also demonstrates that bornite phase are actually intermediate members of the bornite-digenite solid solution (*bdss*), with lower reaction temperatures favoring Cu-rich compositions. The difference of this reaction from the replacement of hematite by bornite is that the presence of U-species did not affect the progress of reactions, even if U-nanoparticles were scavenged as a rim between parent grains and overgrowth areas.

Exsolution textures were observed after an annealing at 150 ^{o}C. Chalcopyrite lamellae in synthetic grains are the product of chalcopyrite exsolution from bornite-digenite solid solution. This is a good example of a back replacement reaction. This work also confirms that fluid can play an important role in exsolution reactions particularly when the overall mineral formation reaction is an interface-coupled dissolution-reprecipitation reaction.

6.3 Observation on the natural uranium-bearing minerals

This Ph.D project also includes observations on the nature uranium-bearing minerals from different U deposits to determine the mineralogical deportment of U in the ores.

In chapter 3, the SEM image of natural sample from Olympic Dam shows the fine grained uraninite with Cu-Fe sulphides, which is similar to our experimental results in this chapter.

At Olympic Dam, uraninite occurs in a wide variety of different textures and associations, suggesting that a number of processes were at play during uranium concentration, including extensive U-scavenging during fluid-mineral interaction. In Chapter 4 a natural sample from Moonta is shown consisting of chalcopyrite lamellae in the bornite matrix. Since the overall volume of the system is contracting, the bornite to chalcopyrite reaction is driven by the loss of Cu to solution rather than the addition of Fe to the system. These observations on natural samples illustrate that our proposed mechanism of exsolution reactions in these system being driven by forms of CDR reactions.

The application of Megapixel-synchrotron X-ray fluorescence (MSXRF) on thin-section scale element mapping at μm-scale spatial resolution and ppm-level detection limits is employed to investigate the element distribution and mobilization in natural samples, in Chapter 5. A large amount of information about the nature and distribution of U from IOCG (Moonta) and sediment-hosted deposits (Lake Frome Embayment) was obtained from about 3.5 hours of MSXRF data collection. The MSXRF map of the Moonta Samples proves that U-enrichment is related to the fluid-mediated replacement of bornite by siderite±hematite. SEM observations show that U occurs mainly as very fine (<<1μm) rims along relict bornite grains, along siderite grains, and in association with chalcopyrite replacing siderite. These textures are strikingly similar to the experimental textures observed during the replacement of hematite by chalcopyrite reported in Chapter 3 and the exsolution of chalcopyrite from bornite digenite solid solution in Chapter 4. In the Lake Frome Embayment samples, the MSXRF maps revealed the complexity of U distribution in the ores at thin section scale and within the orebody. This information is key in assessing the methods for in-situ recovery of metals. MSXRF maps also trace the location of deleterious elements such as As, and

provides the background for assessing element mobility and toxicity in the waste material from mining.

Chapter 5 also reveals other new results for the other deposits studied using MSXRF mapping image analysis, e.g. (i) the distribution of μm-sized Pt-rich grains and Ti-mobility during the formation of schistosity at the Fifield Pt prospect; (ii) confirmation of the two-stage Ge-enrichment in the Barrigão deposit, with demonstration of the presence of Ge in solid solution in the early-formed chalcopyrite; and (iii) the presence of Ge contained in organic matter and of Hg minerals associated with quartzite clasts in the Lake Frome U ores.

6.4 Future work

This Ph.D project focuses on the mechanisms of U scavenging during mineral replacement in the Fe-Cu-S system; and explores the application of advanced technologies to ore petrology. However, during these studies, a number of interesting questions related to the study could not be fully resolved in this thesis. Thus, some relevant future investigations are listed below.

6.4.1 Uranium scavenging during other mineral replacement reactions

The replacement of hematite by magnetite

It is believed that the presence of an oxidizing or reduction agent could drive the transformation of iron oxides in nature. Chapter 3 also indicates that uraninite can be a reduction agent to form magnetite from hematite ores. However, Ohmoto (2003) suggests the mechanism of the iron oxides transformation is the addition or leaching of Fe^{2+} by hydrothermal fluids. The mechanism of transformation from hematite to magnetite could be related to the dissolution of hematite into Fe^{2+} and the reaction between hematite and Fe^{2+} in fluid media. The current understanding is that uraninite is more strongly associated with

hematite than non-hematite gangue or sulphides. Thus, it is also worth exploring different U sources in this system to investigate whether U scavenging or the influence of U on replacement reactions.

The replacement of bornite by siderite±hematite

This thesis investigates the effect of uranyl-bearing fluids on the precipitation of fine-grained uraninite in Fe-oxide/sulfide assemblages. In the case of natural samples from Moonta, U-enrichment is related to the fluid-mediated replacement of bornite by siderite±hematite. On the basis of the formation of copper iron sulfides under hydrothermal conditions carried out in this study, a more fundamental understanding about physical chemistry properties of copper iron sulfides could be extrapolated to study the replacement of bornite by siderite±hematite. Furthermore, following on from the experimental study on U-scavenging in this thesis, different U sources/species could be used into this mineral replacement model, which could help us to clarify the distribution and formation of uranium minerals in the oxidizing environment.

6.4.2 Synthesis of brannerite under hydrothermal conditions

Brannerite (UTi_2O_6) exists naturally in many uranium ore bodies, and is one of the dominant uranium minerals at Olympic Dam. Some important observations have been made for brannerite from previous studies, which were performed at 25 to 35 ^{o}C and 1 atm: (1) brannerite has a low solubility than uraninite in sulphuric acid, (2) coffinite ($U[SiO_4]_{1-x}[OH]_{4x}$) is commonly an alteration product intergrown with brannerite, and (3) brannerite is often associated with rutile and in some cases with anatase as a natural alteration product (Zhang et al., 2003).

The synthesis of brannerite can be achieved by at least two methods. The first route is to heat the mixture of uranium oxide and titanium oxide in argon at more than 1000 ^{o}C. Kaiman (1959) produced the brannerite at 1400 ^{o}C utilising the molecular proportions UO_2/TiO_2=1:2 and 1:2.5 for 90 minutes. This process generated U_3O_8 which resulted in an ignition product of UO_2 and TiO_2 under high temperature, reducing the overall yield of UTi_2O_6. In order to prevent the formation of U_3O_8, carbon was added as a reductant. Patchett and Nuffield (1960) synthesized brannerite by mixing very pure tetravalent uranium oxide with reagent grade TiO_2 in the atomic proportion 1 to 2. This was finely ground, pressed into a pellet, and sintered at a low vacuum in a graphite container at 900 ˚C for eighteen hours (Patchett and Nuffield, 1960). In this system, the use of graphite and synthesis at lower temperature was effective at maintaining the valence state of uranium; however, a much longer reaction time was required due to the reduction in temperature.

Another method of brannerite synthesis was named the alkoxide/nitrate route (Zhang et al., 2011). Stoichiometric mixture of aqueous uranyl nitrate and ethanolic titanyl isopropoxide solution (molecular proportion=1:2) were dried and calcined in argon at 750 ^{o}C for 1hour. The calcines were wet-milled for 2 hours and then dried. 2 wt% of Ti metal was added and sample was hot pressed at 1260 ^{o}C for 2 hours under 21 MPa in graphite dies. The product of this method consisted mainly brannerite with 5-7% of rutile and trace amounts of UO_2 (Zhang et al., 2011). For the alkoxide/nitrate route, the important difference from the first route is the valence of uranium in starting materials. Reaction between uranyl nitrate and titanyl isopropoxide occurred in the starting solution; then U^{6+} was reduced U^{4+} by graphite. Furthermore, the solution reaction also avoids the danger associated with uranium dioxide heated at high temperature (～1000 ˚C). However, it is obvious that all brannerite synthesis

methods developed so far were performed in dry system with a high temperature final step (around 1000 ˚C), and require a reducing agent to be present.

Some papers also mention that pure UTi_2O_6 can only be synthesized by dry ceramic techniques under low-oxygen conditions, and it is clear that incorporation of other impurity ions provides a means of stabilizing the brannerite phase produced in air. The formation of $U_{1-x}M_xTi_2O_6$ brannerite phase in both air and argon with a wide range of ionic substitutions (M=Ca, La, Gd, Y, Hf and Pu) has been reported. Brannerites were stabilized at high temperature by substitution of Ca^{2+}, La^{3+}, or Gd^{3+} for U^{4+} (James and Watson, 2002) .

Brannerite forms at temperatures ≤500 ^oC from hydrothermal fluids in nature, but no study has yet attempted to synthesize brannerite under hydrothermal conditions. Based on the association of brannerite and rutile (anatase) in nature, the formation of brannerite may be related to the mineral replacement reaction between titanium oxide and U-bearing solutions. The results could be important in the understanding of brannerite distribution and the improvement of U mining and processing industry, particularly with regard to leaching and hydrometallurgical processing.

6.5 References

James, M., and Watson, J., 2002, The synthesis and crystal structure of doped uranium brannerite phases U 1− x M x Ti 2 O 6 (M= Ca 2+, La 3+, and Gd 3+): Journal of Solid State Chemistry, v. 165, p. 261-265.

Kaiman, S., 1959, Synthesis of brannerite: Canadian, v. 6, p. 389-390.

Ohmoto, H., 2003, Nonredox transformations of magnetite-hematite in hydrothermal systems: Economic Geology, v. 98, p. 157-161.

Patchett, J., and Nuffield, E., 1960, Studies of radioactive compounds. X. The synthesis and crystallography of brannerite: Canad. Mineral., v. 6.

Zhang, F., Lang, M., Liu, Z., and Ewing, R. C., 2011, Phase stability of some actinides with brannerite structure at high pressures: Journal of Solid State Chemistry, v. 184, p. 2834-2839.

Zhang, Y., Thomas, B., Lumpkin, G., Blackford, M., Zhang, Z., Colella, M., and Aly, Z., 2003, Dissolution of synthetic brannerite in acidic and alkaline fluids: Journal of nuclear materials, v. 321, p. 1-7.

Zhao, J., Brugger, J., Chen, G., Ngothai, Y., and Pring, A., 2014, Experimental study of the formation of chalcopyrite and bornite via the sulfidation of hematite: Mineral replacements with a large volume increase: American Mineralogist, v. 99, p. 343-354.

Appendix A

Geobiology of in situ uranium leaching

Statement of Authorship

Title of Paper	Geobiology of *in situ* uranium leaching
Publication Status	Published
Publication Details	Zammit, C., K. Li, B. Etschmann, J. Brugger and F. Reith (2013). Geobiology of in situ uranium leaching. Advanced Materials Research, Trans Tech Publ.

Principal Author

Name of Principal Author	Carla Zammit		
Contribution to the Paper	Designed and performed experiments, interpreted and processed data, wrote manuscript. Acted as cooresponding author.		
Overall percentage (%)	70%		
Signature		Date	10 September 2015

Co-Author Contributions

By signing the Statement of Authorship, each author certifies that:

i. the candidate's stated contribution to the publication is accurate (as detailed above);
ii. permission is granted for the candidate in include the publication in the thesis; and
iii. the sum of all co-author contributions is equal to 100% less the candidate's stated contribution.

Name of Co-Author	Kan Li		
Contribution to the Paper	Performed experiments		
Signature		Date	10 September 2015

Name of Co-Author	Barbara Etschmann		
Contribution to the Paper	Helped in data interpretation and manuscript evaluation.		
Signature		Date	09 September 2015

!

Name of Co-Author	Joël Brugger		
Contribution to the Paper	Superivsed development of work, helped in data interpretation and manuscript evaluation.		
Signature		Date	09 September 2015

Name of Co-Author	Frank Reith		
Contribution to the Paper	Superivsed development of work, helped in data interpretation and manuscript evaluation.		
Signature		Date	07 September 2015

!

Zammit, C., Li, K., Etschmann, B., Brugger, J. & Reith, F. (2013). Geobiology of in situ uranium leaching.
Advanced Materials Research, 825, 372-375.

Appendix B

Microporous gold: Comparison of textures from nature and experiments

Statement of Authorship

Title of Paper	Microporous gold: Comparison of textures from nature and experiments
Publication Status	Published
Publication Details	Okrugin, V. M., E. Andreeva, B. Etschmann, A. Pring, K. Li, J. Zhao, G. Griffiths, G. R. Lumpkin, G. Triani and J. Brugger (2014). "Microporous gold: Comparison of textures from Nature and experiments." American Mineralogist 99(5-6): 1171-1174.

Principal Author

Name of Principal Author	Victor M. Okrugin		
Contribution to the Paper	Collected nature samples, interpreted and processed data, wrote manuscript.		
Overall percentage (%)	70%		
Signature		Date	16 September 2015

Co-Author Contributions

By signing the Statement of Authorship, each author certifies that:

i. the candidate's stated contribution to the publication is accurate (as detailed above);
ii. permission is granted for the candidate in include the publication in the thesis; and
iii. the sum of all co-author contributions is equal to 100% less the candidate's stated contribution.

Name of Co-Author	Elena Andreeva		
Contribution to the Paper	Collected nature samples and manuscript evaluation.		
Signature		Date	16 September 2015

Name of Co-Author	Barbara Etschmann		
Contribution to the Paper	Designed and performed experiments. Helped in data interpretation and manuscript evaluation.		
Signature		Date	16 September 2015

Name of Co-Author	Allan Pring		
Contribution to the Paper	Superivsed development of work, helped in data interpretation and manuscript evaluation.		
Signature		Date	13 September 2015

Name of Co-Author	Kan Li		
Contribution to the Paper	Designed and performed experiments. Helped in data interpretation and manuscript evaluation.		
Signature		Date	16 September 2015

Name of Co-Author	Jing Zhao		
Contribution to the Paper	Designed and performed experiments. Helped in data interpretation and manuscript evaluation.		
Signature		Date	16 September 2015

Name of Co-Author	Daryl Howard		
Contribution to the Paper	Help in data interpretation and manuscript evalution.		
Signature		Date	10 September 2015

Name of Co-Author	Grant Griffiths		
Contribution to the Paper	Designed and performed experiments. Helped in data interpretation and manuscript evaluation.		
Signature		Date	20 September 2015

Name of Co-Author	Gergory R. Lumpkin		
Contribution to the Paper	Designed and performed experiments. Helped in data interpretation and manuscript evaluation.		
Signature		Date	18 September 2015

Name of Co-Author	Gerry Triani		
Contribution to the Paper	Designed and performed experiments. Helped in data interpretation and manuscript evaluation.		
Signature		Date	18 October 2015

Name of Co-Author	Joël Brugger		
Contribution to the Paper	Superivsed development of work. Designed and performed experiments. Helped in data interpretation and manuscript evaluation.helped in data interpretation and manuscript evaluation, and acted as cooresponding author.		
Signature		Date	16 September 2015

Okrugin, V.M., Andreeva, E., Etschmann, B., Pring, A., Li, K., Zhao, J., Griffiths, G., Lumpkin. G.R., Triani, G. & Brugger, J. (2014). Microporous gold: Comparison of textures from nature and experiments,
American Mineralogist, 99(5-6), 1171-1174.

Appendix C

Hydrothermal mineral replacement reactions and their applications in mining and processing

Statement of Authorship

Title of Paper	Hydrothermal mineral replacement reactions and their applications in mining and processing
Publication Status	Published
Publication Details	Zhao, J., A. Pring, J. Brugger, F. Xia, K. Li and Y. Ngothai (2013). Hydrothermal mineral replacement reactions and their applications in mining and processing. International Seminar on Process Hydrometallurgy (5th: 2013: Santiago, Chile).

Principal Author

Name of Principal Author	Jing Zhao		
Contribution to the Paper	Designed and performed experiment, interpreted and processed data, wrote manuscript		
Overall percentage (%)	70%		
Signature		Date	10 September 2015

Co-Author Contributions

By signing the Statement of Authorship, each author certifies that:

i. the candidate's stated contribution to the publication is accurate (as detailed above);
ii. permission is granted for the candidate in include the publication in the thesis; and
iii. the sum of all co-author contributions is equal to 100% less the candidate's stated contribution.

Name of Co-Author	Allan Pring		
Contribution to the Paper	Superivsed development of work, helped in manuscript evaluation.		
Signature		Date	12 September 2015

Name of Co-Author	Joël Brugger		
Contribution to the Paper	Superivsed development of work, helped in data interpretation and manuscript evaluation.		
Signature		Date	10 September 2015

Name of Co-Author	Fang Xia		
Contribution to the Paper	Helped to evaluate and edit the manuscript.		
Signature		Date	10 September 2015

Name of Co-Author	Kan Li		
Contribution to the Paper	Helped to evaluate and edit the manuscript.		
Signature		Date	11 September 2015

Name of Co-Author	Yung Ngothai		
Contribution to the Paper	Superivsed development of work and helped in manuscript evaluation.		
Signature		Date	11 September 2015

!

Zhao, J., Pring, A., Brugger, J., Xia, F., Li, K. & Ngothai, Y. (2013). Hydrothermal mineral replacement reactions and their applications in mining and processing. *5th International Seminar on Process Hydrometallurgy*, Santiago, Chile.